ISM and HII regions in extreme starbursts

Ángel R. López-Sánchez

School of Mathematical and Physical Sciences, FSE, Macquarie University

BlueMUSE Workshop – Online – 23 Apr 2024

MACQUARIE University
SYDNEY·AUSTRALIA

MACQUARIE University
Astrophysics and Space Technologies Research Centre

Extreme starbursts: the large majority are Blue Compact Dwarf Galaxies (BCDGs)

- Subset of **low-luminosity** ($M_B \geq -18$) and **low metallicity** (~10% solar) galaxies undergoing a **strong** and **short-lived** episode of **star formation**.
- Quickly gas consumption.
- **Compact**, **irregular** morphologies.
- Intense **narrow emission lines** superposed on a **blue continuum**.
- The **starbust** and a **very young stellar population** dominate the optical light (Cairós et al. 2001), very often masking all evidence of the **underlying older stellar population** (Noeske et al. 2003).
- What is the **origin** and **nature** of their starburt activity?
- They offer a **unique** opportunity to study galaxy formation under conditions approaching those of the **first galaxies**, prior to and during the epoch of reionization (EoR).

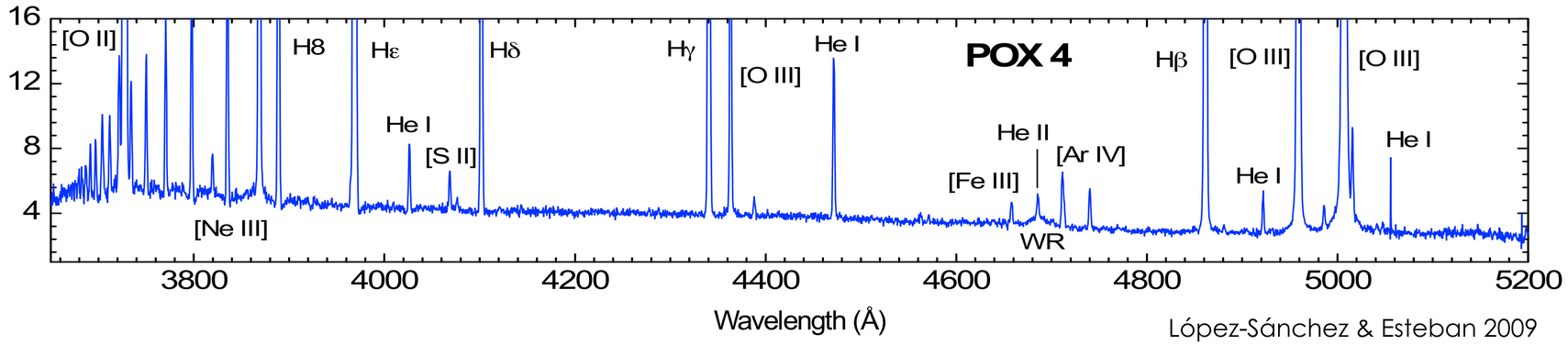

López-Sánchez & Esteban 2009

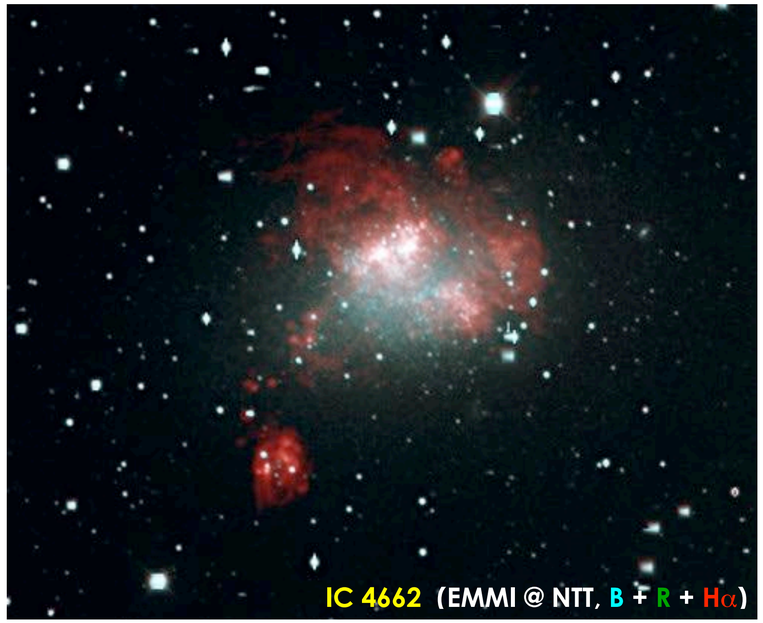

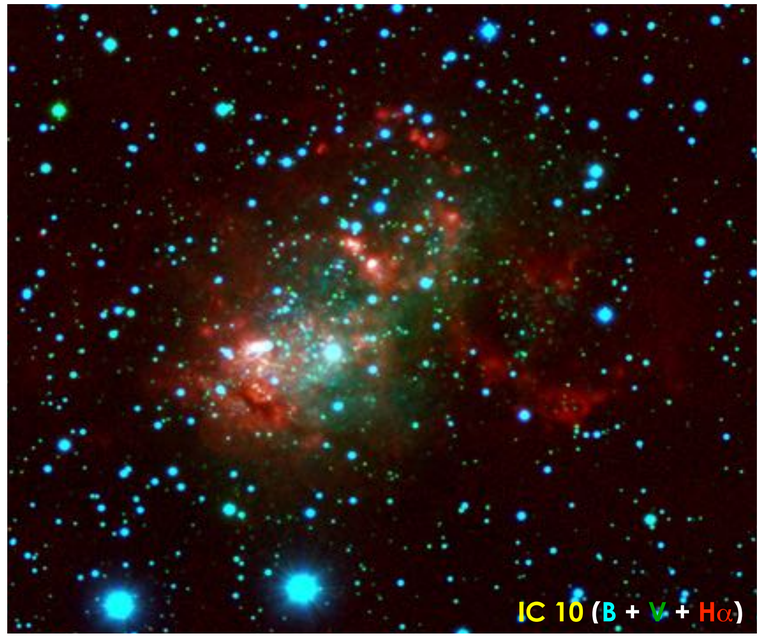

Ángel R. López-Sánchez @El_Lobo_Rayado

Local extreme starburts: unique laboratories to explore dwarf galaxy formation and evolution

- Allow us to study in detail the **physical** and **chemical** properties of the ISM of dwarf galaxies.
- Enable detailed studies of star formation (including **feeding** / **triggering** mechanisms) and the associated **feedback** processes in the least chemically evolved local environments known (Kunth & Ostlin, 2000; James et al. 2015)
- Allow us studies of the most rare, **massive and extreme stars** (including Wolf-Rayet stars) at low intrinsic extinction (Crowther & Bibby, 2009; Kehrig et al. 2015)
- Are likely the sites of super-luminous **supernova/hypernova explosions** (Leloudas et al. 2015) and long-duration GRBs (Hashimoto et al. 2015)
- their shallow gravitational potential wells provide less resistance to **galactic outflows**, enriching the intergalactic medium with metals (Cameron et al. 2022; Hamel-Bravo et al. 2024)
- The **chemical abundance patterns** in BCDGs (Roy & Kunth, 1995) can place valuable constraints on the timescales for dispersal and mixing of heavy elements in protogalaxies;
- they have more porous/disrupted ISM, which enhances the **escape of Lyman-radiation and ionizing continua**. This allow us to understand how similar galaxies at high-redshift leak ionizing photons, reionise the Universe, and maintain the meta-galactic ionizing background.
- they may be the **closest analogues** of some of the faint galaxies identified in high-z surveys, that dominate the star-formation budget at early times
- some of the most metal-poor —12+log(O/H) < 7.6 — local BCDGs have experienced the dominant phase of their build-up **at a late cosmic epoch**

Ángel R. López-Sánchez @El_Lobo_Rayado

Local extreme starburts: unique laboratories to explore dwarf galaxy formation and evolution

- Allow us to study in detail the **physical** and **chemical** properties of the ISM of dwarf galaxies.
- Enable detailed studies of star formation (including **feeding** / **triggering** mechanisms) and the associated **feedback** processes in the least chemically evolved local environments known (Kunth & Ostlin, 2000; James et al. 2015)
- Allow us studies of the most rare, **massive and extreme stars** (including Wolf-Rayet stars) at low intrinsic extinction (Crowther & Bibby, 2009; Kehrig et al. 2015)
- Are likely the sites of super-luminous **supernova/hypernova explosions** (Leloudas et al. 2015) and long-duration GRBs (Hashimoto et al. 2015)
- their shallow gravitational potential wells provide less resistance to **galactic outflows**, enriching the intergalactic medium with metals (Cameron et al. 2022; Hamel-Bravo et al. 2024)
- The **chemical abundance patterns** in BCDGs (Roy & Kunth, 1995) can place valuable constraints on the timescales for dispersal and mixing of heavy elements in protogalaxies;
- they have more porous/disrupted ISM, which enhances the **escape of Lyman-radiation and ionizing continua**. This allow us to understand how similar galaxies at high-redshift leak ionizing photons, reionise the Universe, and maintain the meta-galactic ionizing background.
- they may be the **closest analogues** of some of the faint galaxies identified in high-z surveys, that dominate the star-formation budget at early times
- some of the most metal-poor —12+log(O/H) < 7.6 — local BCDGs have experienced the dominant phase of their build-up **at a late cosmic epoch**

Ángel R. López-Sánchez @El_Lobo_Rayado
MACQUARIE University

Metals: Connecting stars and gas to understand galaxy evolution

- Metals is a way of measuring **HOW MUCH THE GAS HAS BEEN PROCESSED INTO STARS**
- Informs about the **star formation history** and **assembly** of galaxies.
- Traces **infalling** of pristine gas... or **outflows** of processed gas.
- Helps to disentangle the **nature** of diffuse objects around galaxies
- Example:
  gas, stars and metals in NGC 1512 / 1510

  – Arm 2 has experienced a larger chemical enrichment that Arm 1.
  – The gas already had **a lot of metals** before the star-formation started!
  – Metals are coming from the **circumgalactic medium**, perhaps from dwarf, low-luminosity, gas-rich galaxies which have been slowly accreted and destroyed into the system.

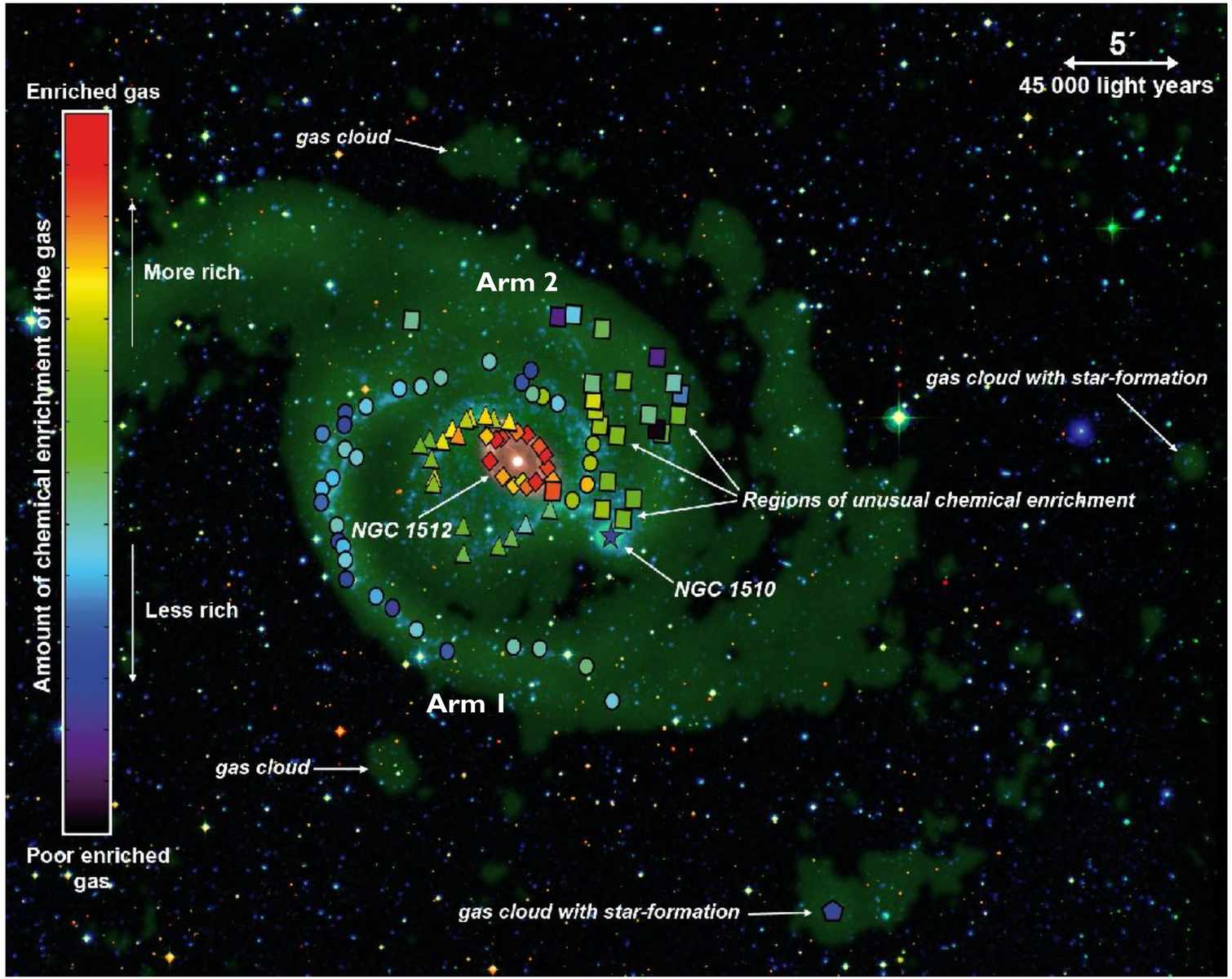

Koribalski & López-Sánchez 2009, MNRAS
López-Sánchez et al. 2015, MNRAS, 450, 3381

Ángel R. López-Sánchez @El_Lobo_Rayado
MACQUARIE University

Malin 1 with MUSE: HII regions, SFR, metallicity, dust attenuation

- Junais et al. (2024)

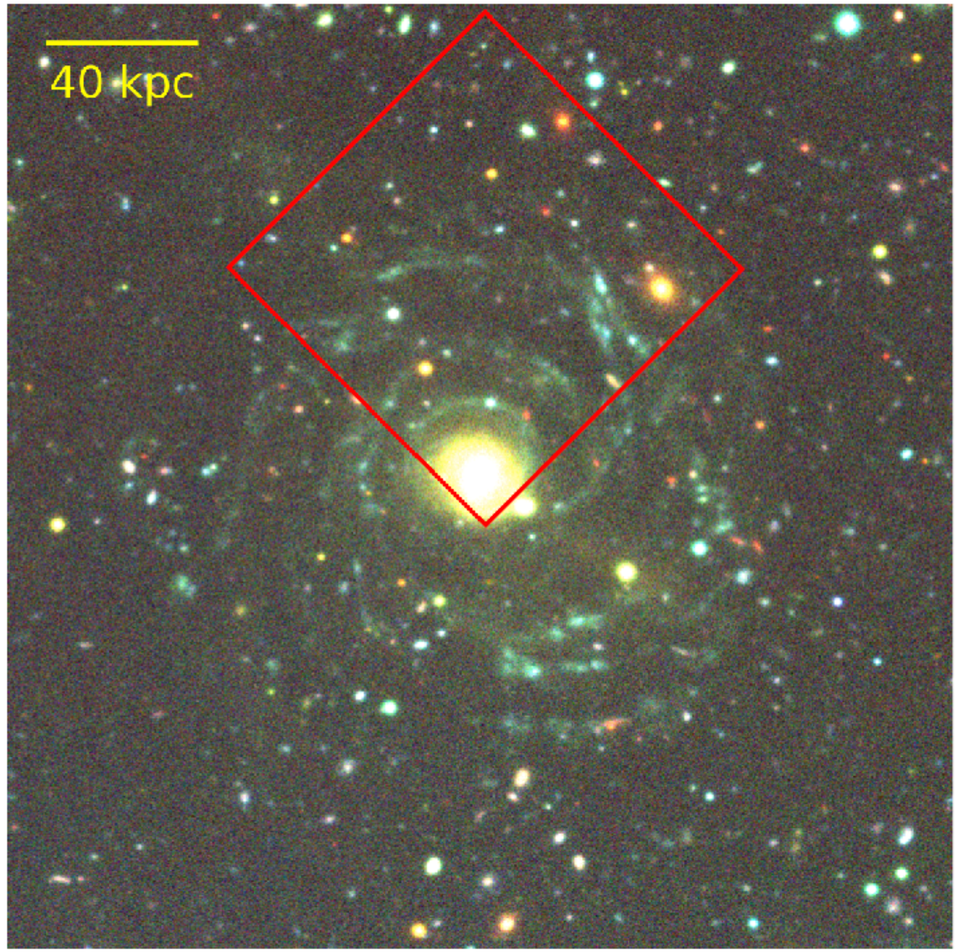

Fig. 1. Color-composite image of Malin 1 from the Canada-France-Hawaii Telescope (CFHT) Megacam NGVS survey *u*-, *g*-, and *i*-band images (Ferrarese et al. 2012). The image spans a width of ~2.6′ × 2.6′. The red box shows the MUSE field of observation (1′ × 1′).

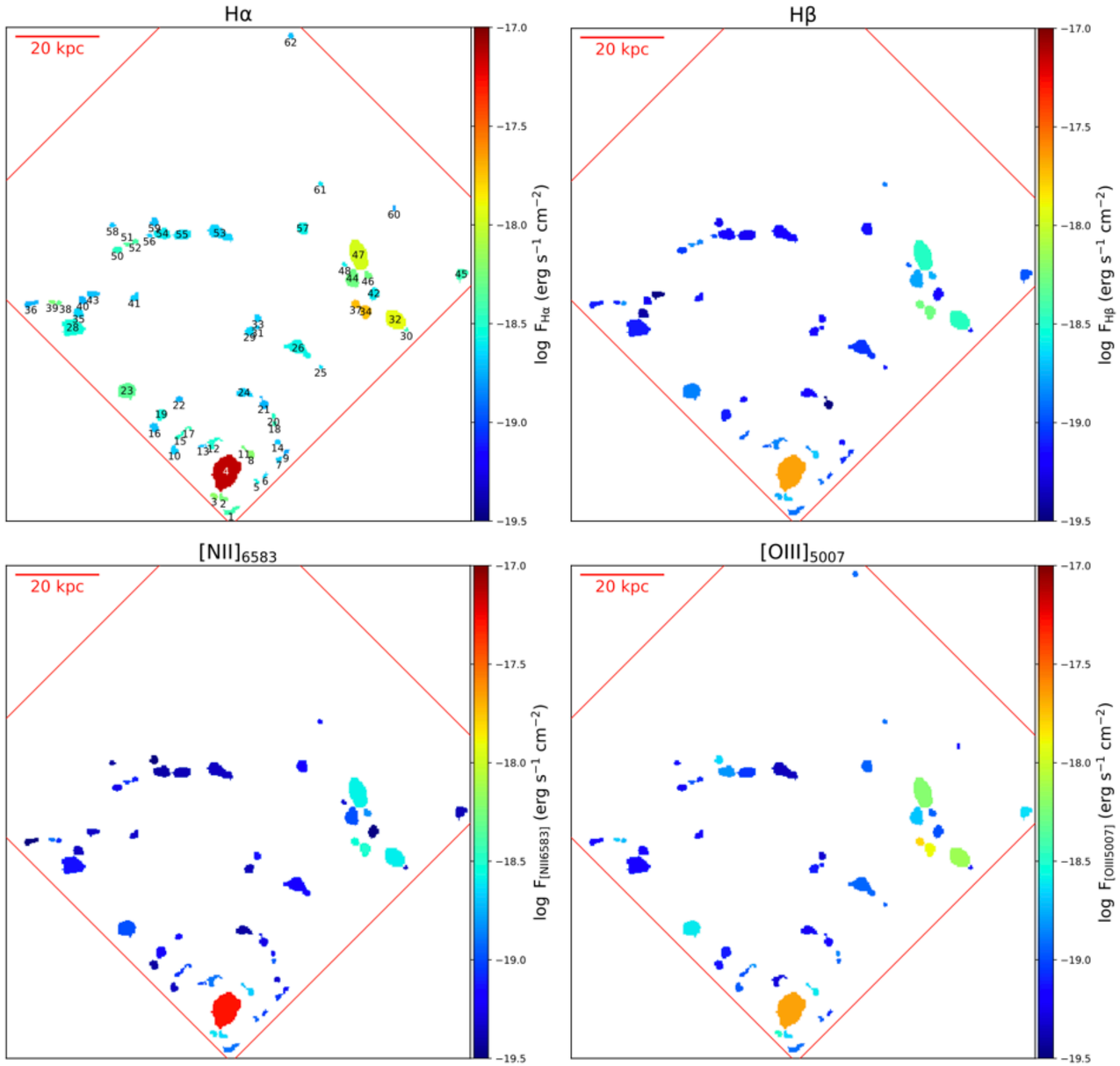

Ángel R. López-Sánchez @El_Lobo_Rayado

A warning about gas-phase metallicities

- **OXYGEN ABUNDANCE**: 12 + log (O / H)

1. The problem of the **ABSOLUTE** scale

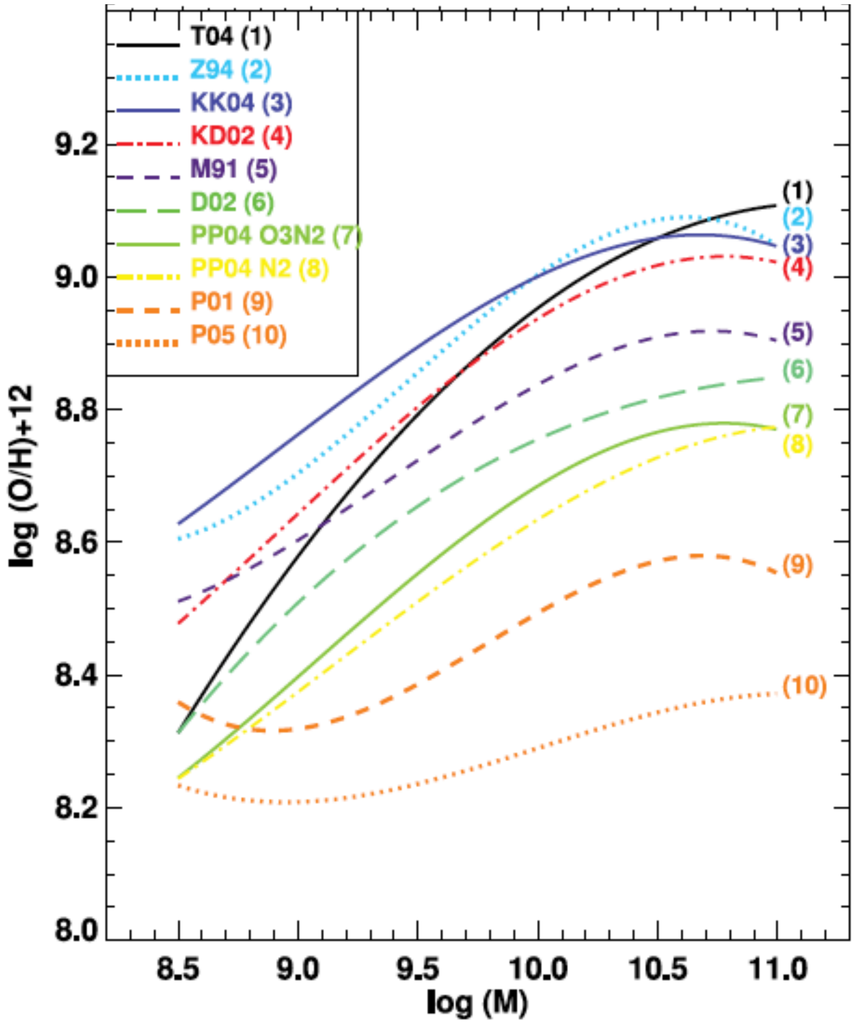

Kewley & Ellison 2008

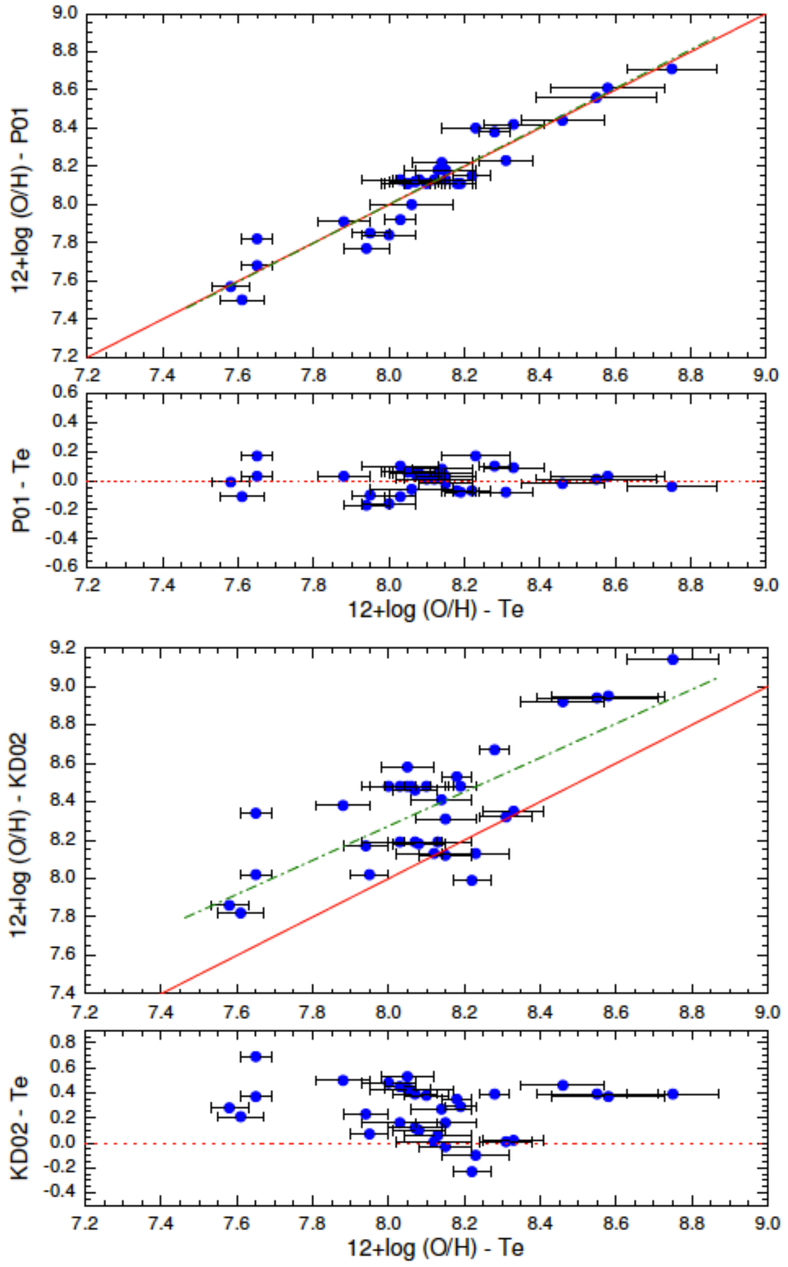

López-Sánchez, PhD (2006)

López-Sánchez & Esteban, 2010b, A&A, 517, 85

López-Sánchez, Dopita, Kewley et al. 2012, MNRAS, 426, 2630

A warning about gas-phase metallicities

- **OXYGEN ABUNDANCE**: 12 + log (O / H)

1. The problem of the **ABSOLUTE** scale
2. **Resolving HII regions** when using IFS data
   - ★ The **ionization structure** plays an important role !
     - Evident when using N2 and O_3N_2
   - ★ IFS analyses of star-forming galaxies needs **observations deep enough to detect the faint auroral lines** (see also James et al. 2009, 2010).
   - ★ **IMPORTANT:** Oxygen abundance maps obtained using empirical calibrations **may show features that are not related with the actual metallicity** distribution of a star-forming galaxy but with the **IONIZATION STRUCTURE** within its giant H II regions.

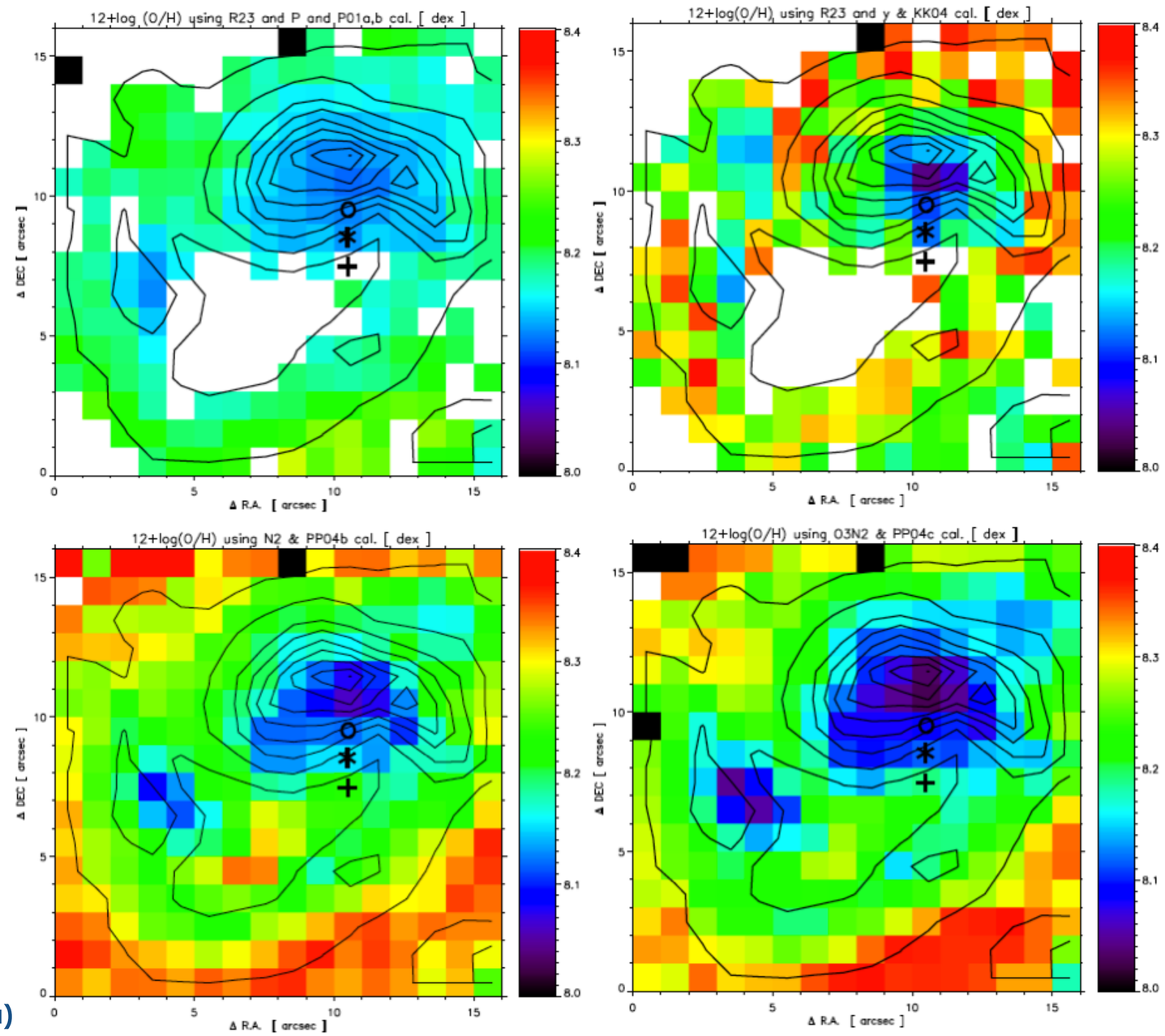

López-Sánchez et al. 2011, MNRAS, 411, 2076 (PMAS data)

Local extreme starburts: observations needed

- Analyse / study both **local** and **global** properties: **IFS data !!**
- **Deep spectra** with at least **moderate** (R~3500) spectral resolution to identify and measure well key features,
- **Blue wavelengths** to get [O II] 3727, [O III] 3727 and the many important features in the 3700 - 4500 A range.
- (**HI data** and other **multi-wavelength** data too).

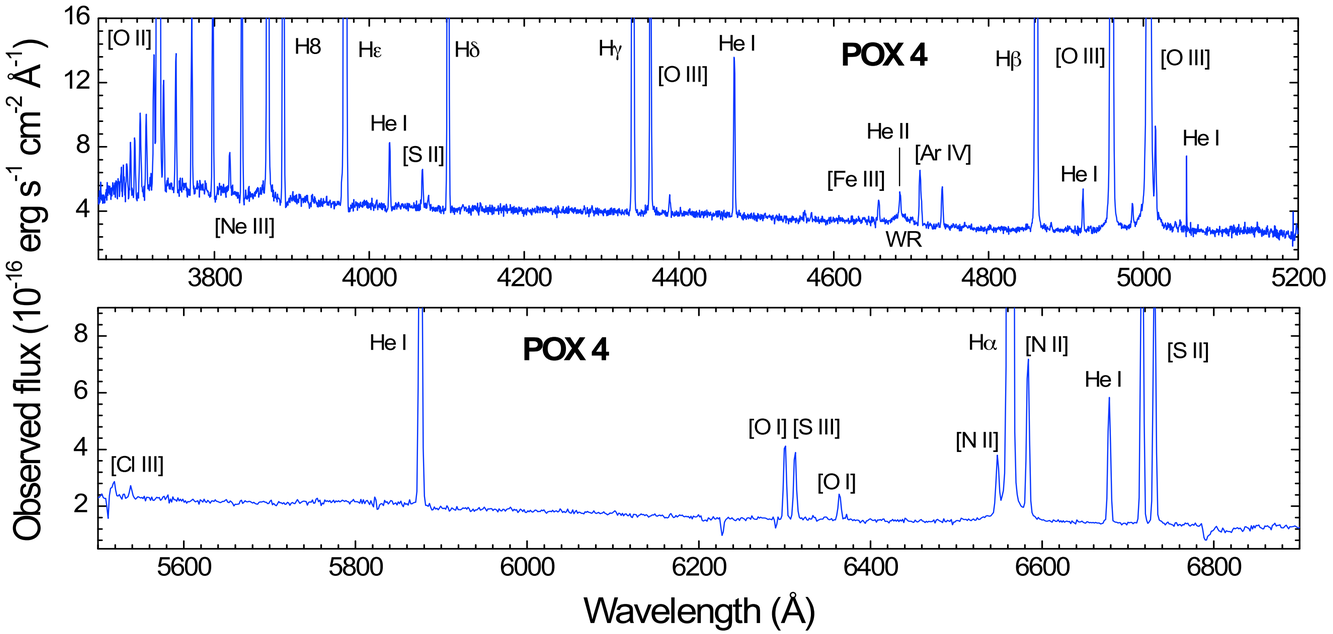

López-Sánchez & Esteban 2009

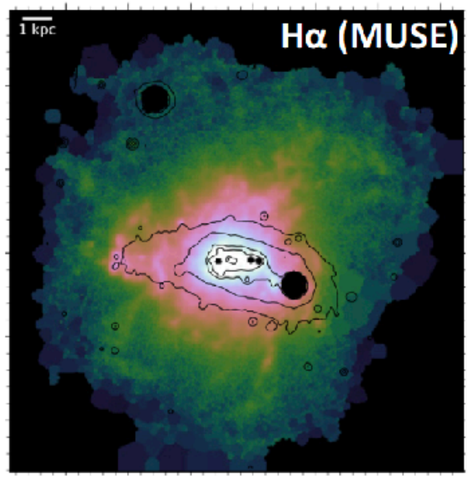

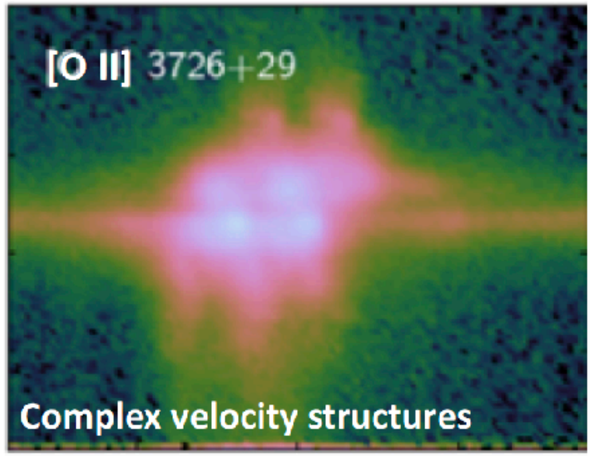

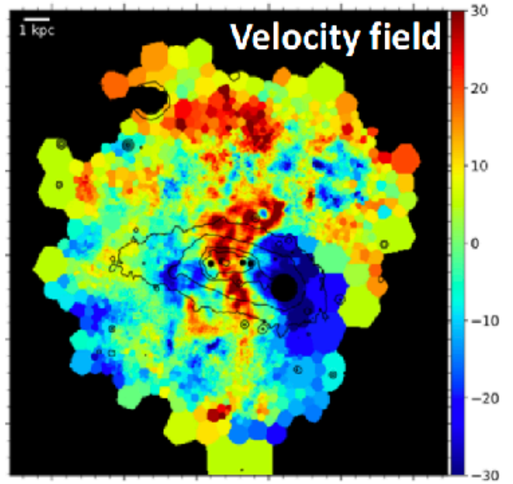

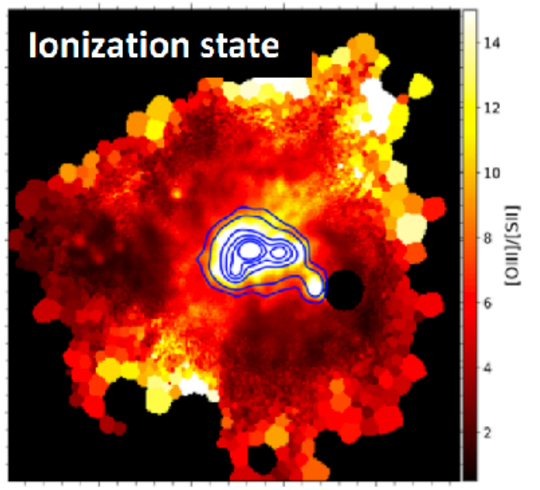

ESO 338-IG04 using MUSE and XSHOOTER (Bik et al 2018)

Gas and metals in the BCDG NGC 5253

López-Sánchez, Esteban, García-Rojas, Peimbert & Rodríguez 2007, ApJ 656, 168

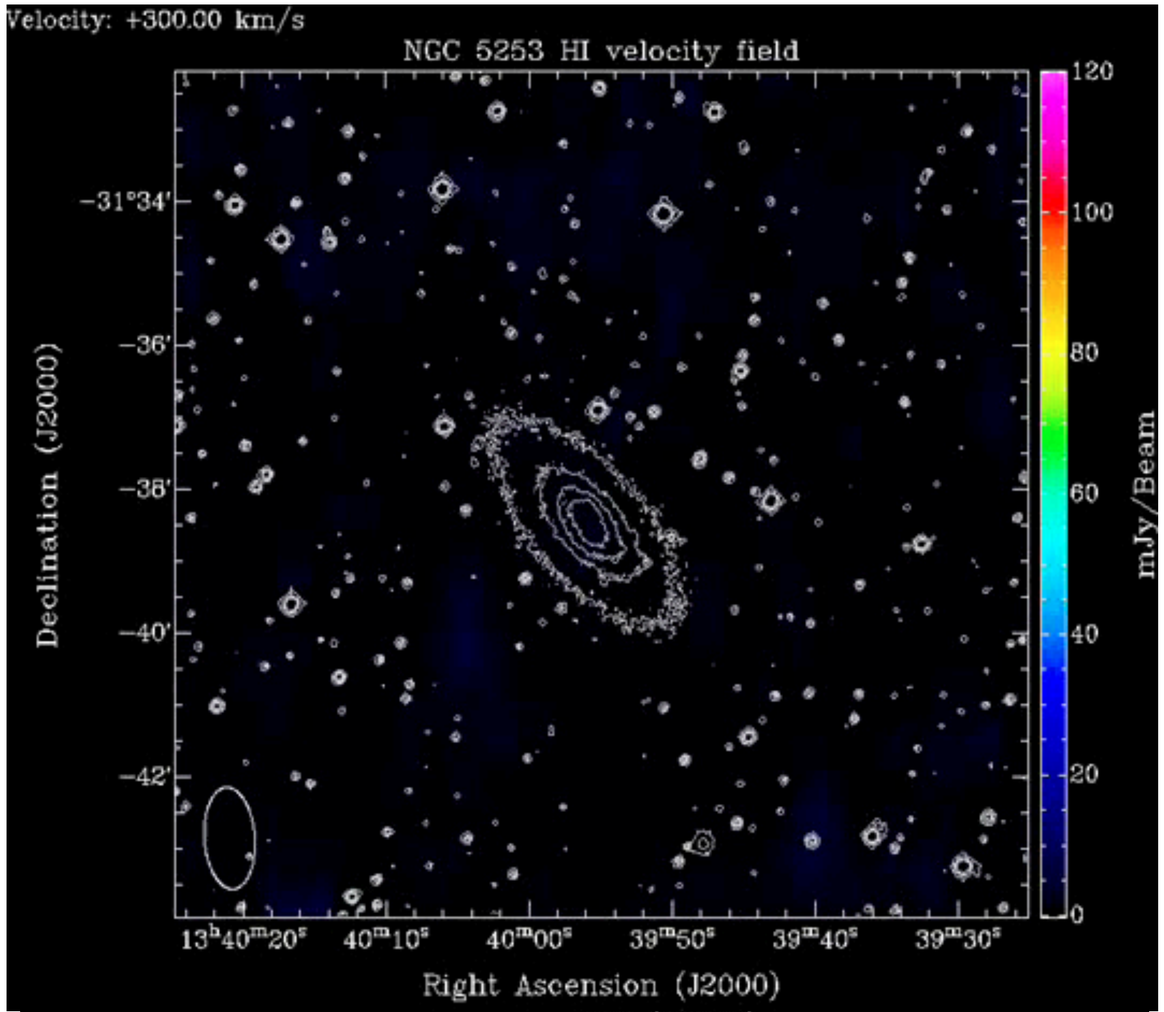

NGC 5253 – Low-resolution H I map (pale blue) + UV (blue) R (green) + Hα (red) + J (orange)

López-Sánchez et al. 2012a, see also Kobulnicky & Skillman 2008

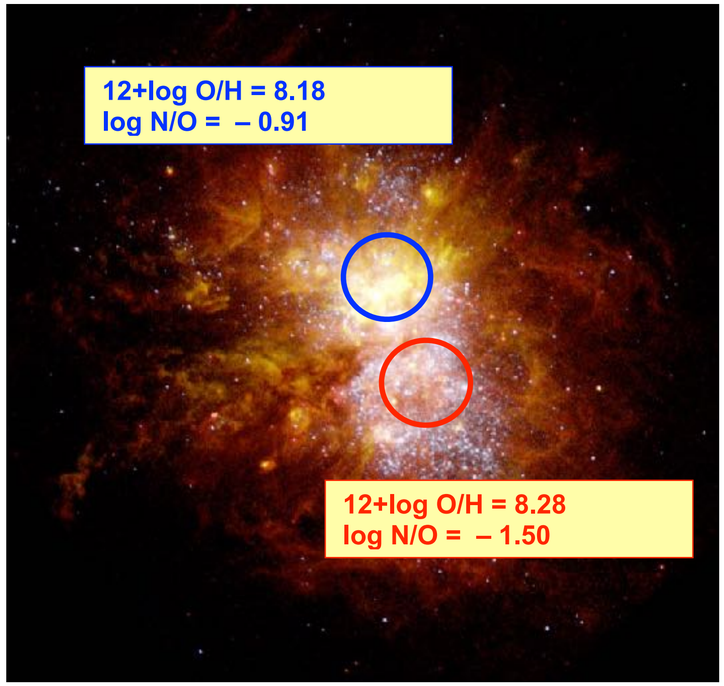

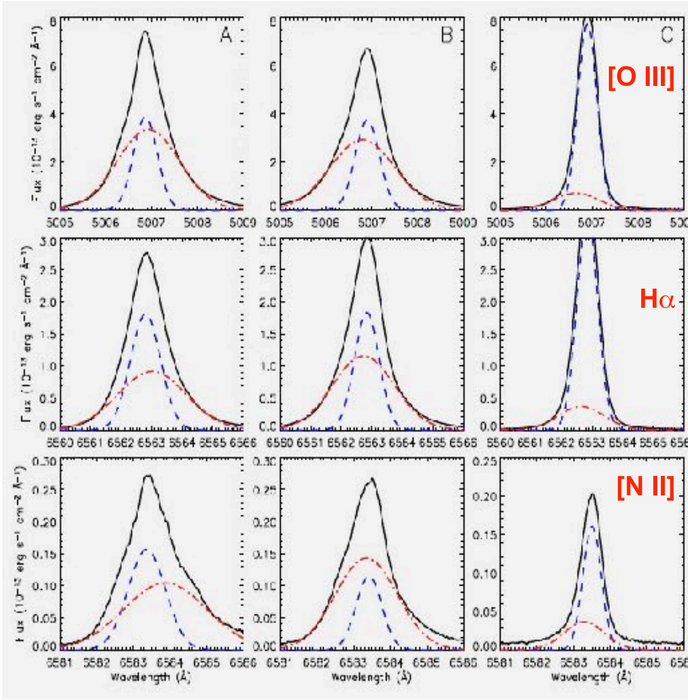

★ Discovery of O II and C II lines: first time in starburst, O/H with them

★ Localized N (& He) enrichment: the broad component has it

López-Sánchez et al. 2007

★ Low M_{gas} / M_{stars} for its O/H (& low O/H for its M_{gas} / M_{stars} ratio)

López-Sánchez et al. 2010

★ Disruption/accretion of a metal-poor gas-rich companion

López-Sánchez et al. 2012

Wolf-Rayet stars in starbursts

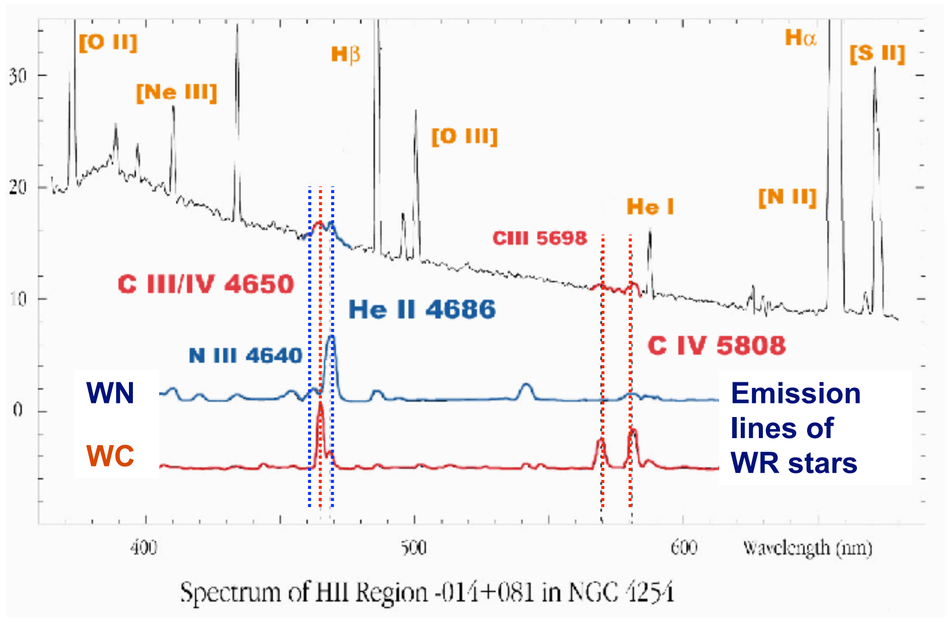

Blue WR Bump ~ 4650 Å
WNL stars

Blue WR Bump ~ 5800 Å
WC stars

– The **number of WR** stars with respect O stars is high, the burst should be **short**.

– **IMF** extended to **HIGH masses**

– **Short-lived starburst** (< 6 Myr)

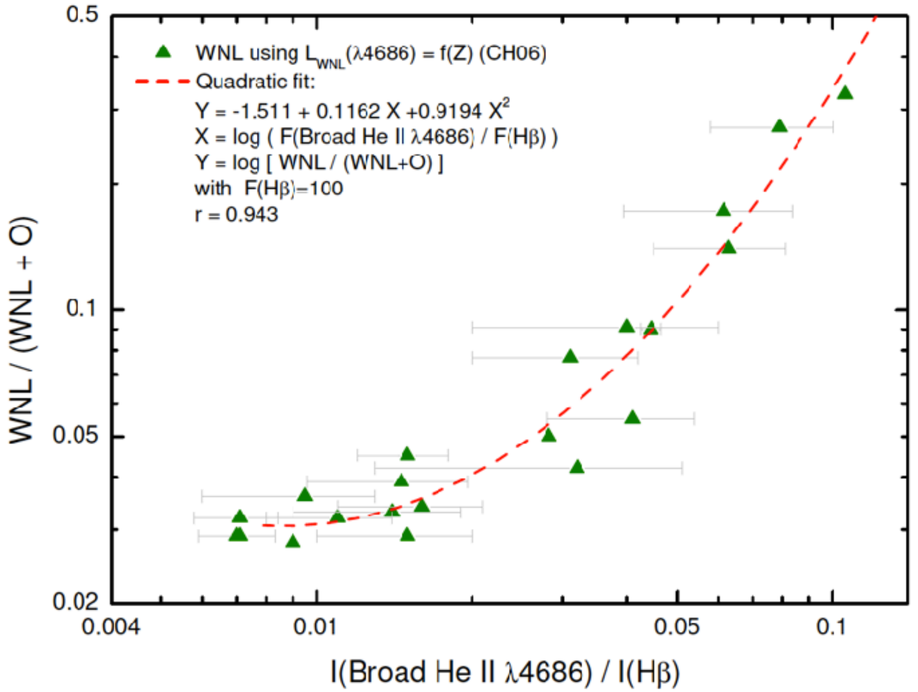

López-Sánchez & Esteban (2009, 2010a)

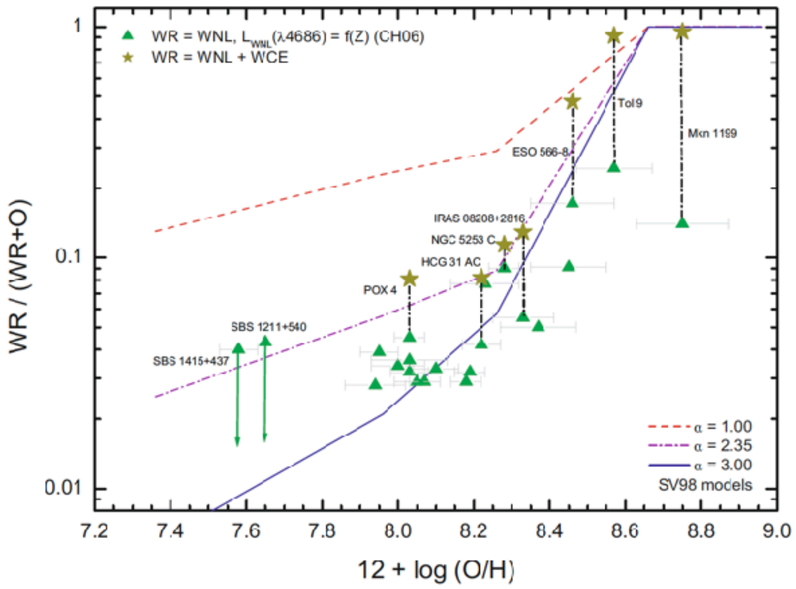

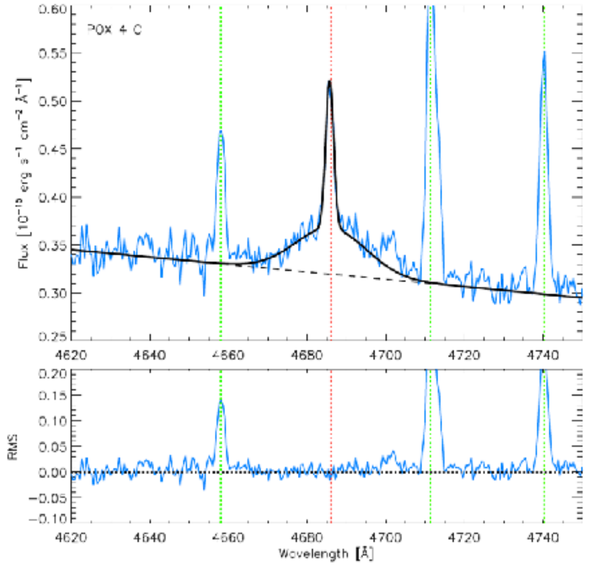

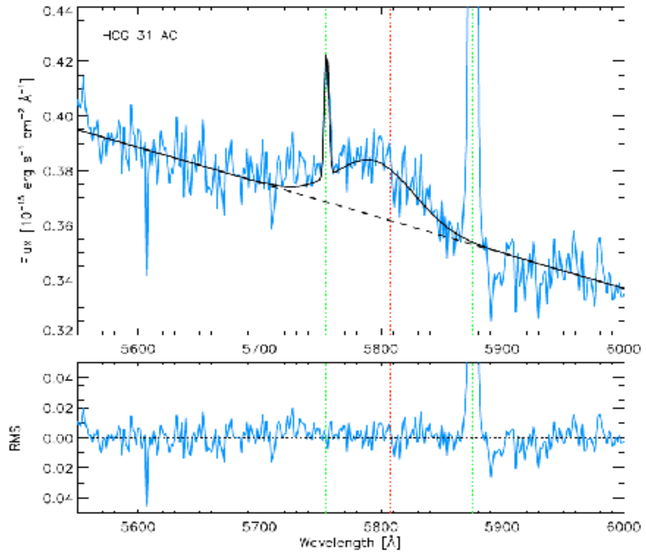

Ángel R. López-Sánchez @El_Lobo_Rayado

Wolf-Rayet features in IC10

- PMAS observations of region [HL90] 111 in IC 10 (López-Sánchez et al. 2011)

- We clearly detect the **blue WR bump** in two adjacent fibers.
  - This position coincides with **WR star [MAC92] 24C** catalogued by Crowther et al. (2003).
  - WR bump essentially constituted by the **stellar, broad, He II λ4686** emission feature
  - C III / C IV λ4650 or the C IV λ5808 (the red WR bump) are not detected:
    - the emission comes from a **WN star.**
  - Because of the strength of the broad He II λ4686 emission and the absence of the N V λ4604 emission
    - That is a **late-type WN star (WNL).**

- We followed **López-Sánchez & Esteban (2010a)** to estimate the flux of the blue WR Bump.
  - We fitted a **broad and a narrow Gaussian** for the stellar and nebular He II λ4686 lines.
  - $L_{He\ II,broad}$ = **$(1.35 \pm 0.17) \times 10^{36}$ erg s^{-1}.**
  - Considering a metallicity-dependence of the WR luminosities **$L_{WNL(He\ II\ \lambda4686)} = 1.27 \times 10^{36}$ erg s^{-1}.**
  - Hence, the blue WR bump observed in this position of IC 10 is consistent with being produced **by a single WNL star !!!**

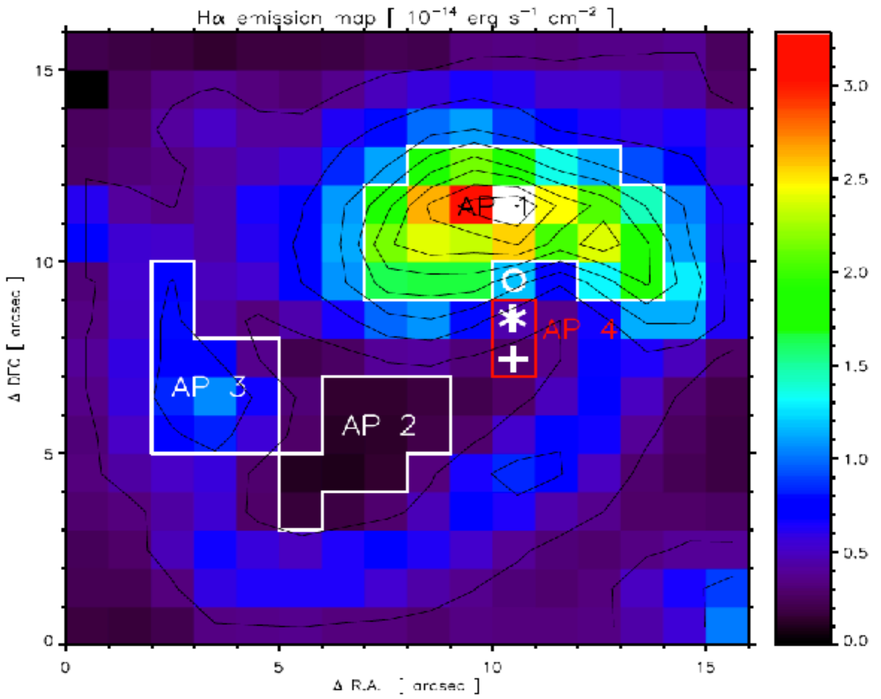

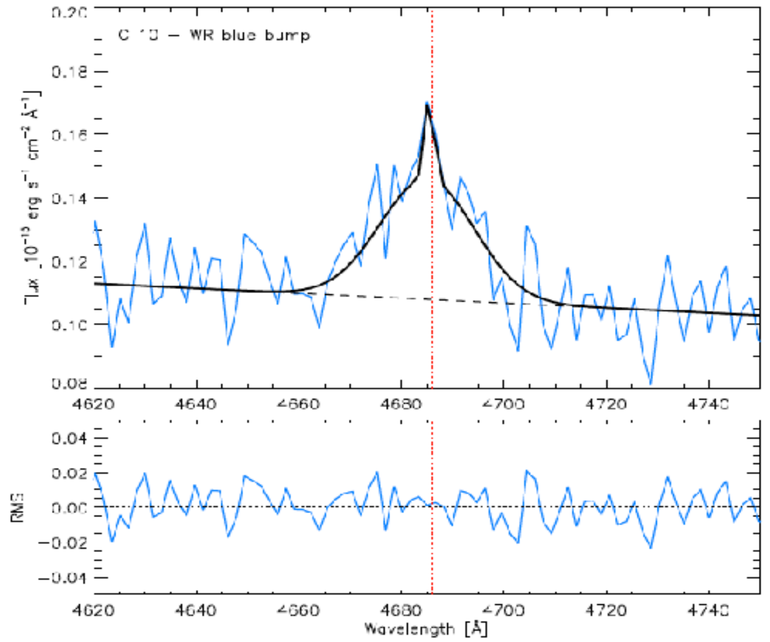

Localized chemical pollution by Wolf-Rayet stars in IC10?

- Our maps suggest the detection of a **localized high N/O ratio at the position** of the WR star !
  - However, we cannot definitively confirm it because of the **relatively high uncertainties**, but all evidence points towards it.
  - The **helium enrichment** is indeed confirmed within the errors.

- Derived **stellar yields agree** with the scenario of chemical pollution by the ejecta of few WR stars.
- If real, this chemical pollution is **very localized** (2" ~7.8 pc), it should be **very difficult to detect in fainter and distant galaxies**.
- Problem of **high N/O ratio** in BCDGs ! (see Pustilnik et al. 2004; López-Sánchez & Esteban 2010b).

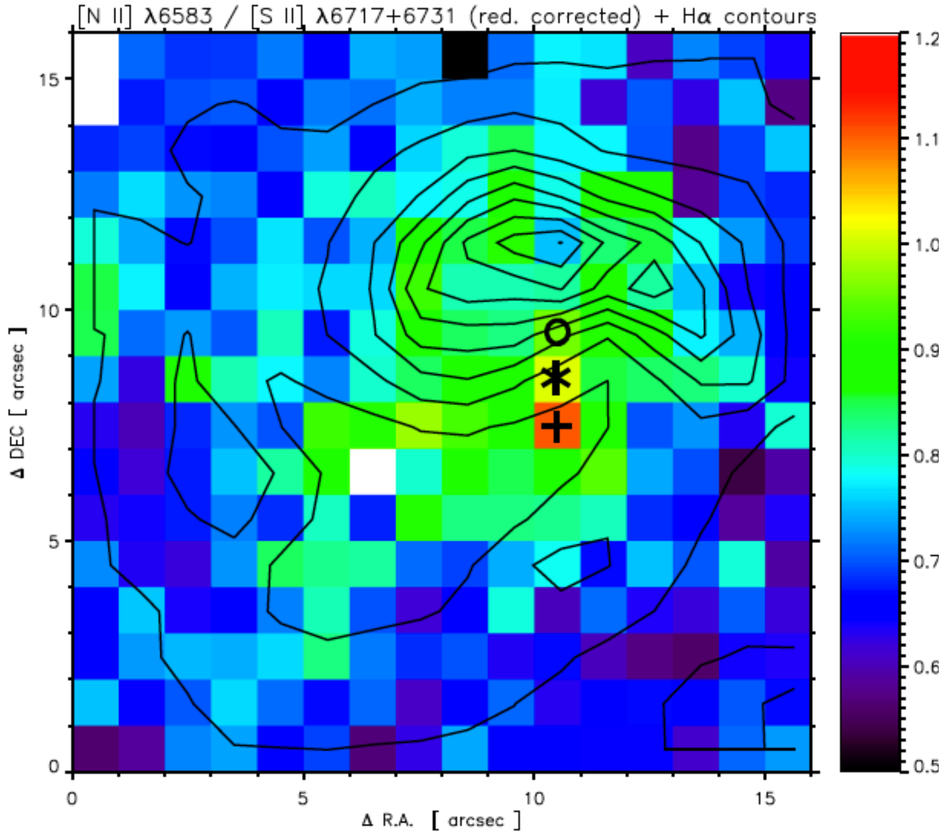

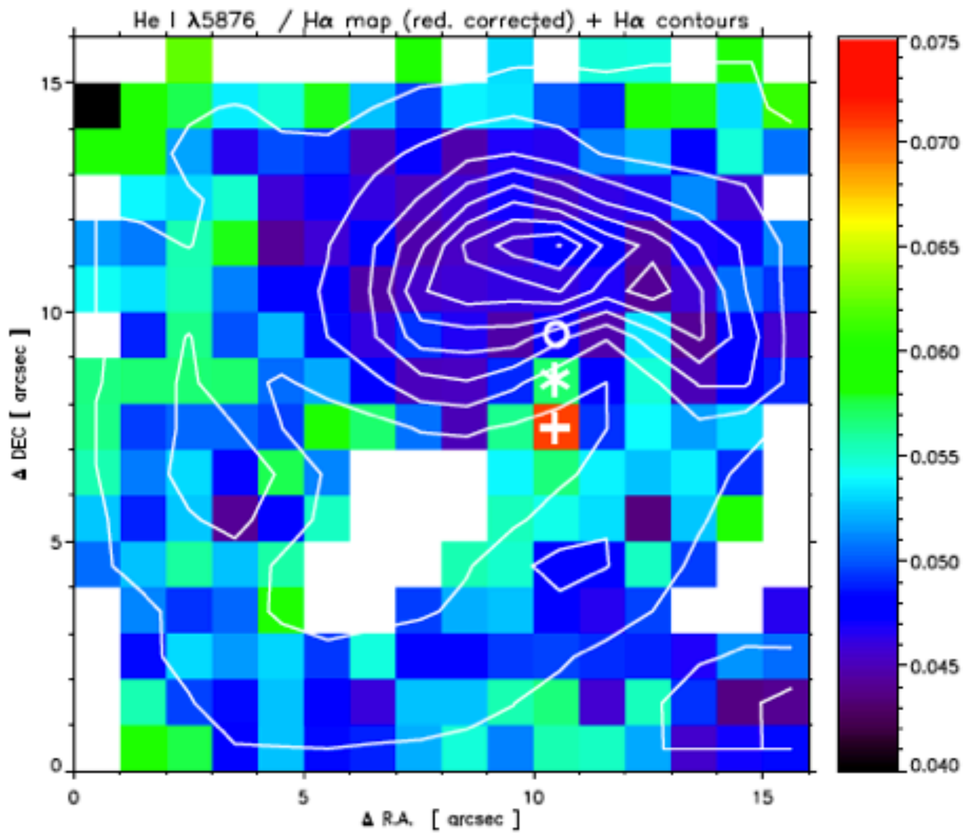

IFU data are fundamental to address these problems in local star-forming galaxies and get clues about the origin of the high N/O ratios and the effect of WR stars in the ISM !!!

Ángel R. López-Sánchez @El_Lobo_Rayado
MACQUARIE University

Stellar feedback in HII regions within nearby, low-metallicity, dwarf galaxies

8. Summary & conclusions

In this paper, we have presented the results of a stellar feedback study of HII regions within three nearby, low-metallicity, dwarf starburst galaxies (J0921, KKH046, and Leo P), which were observed with the IFU spectrograph, MUSE, and collected by the DWALIN collaboration. We have discussed the methods used to select and extract the integrated spectra of these HII regions via the ASTRODENDRO Python package, and the methods used to derive their key ionised gas properties. We have also presented the use of stochastically sampled stellar population synthesis models using the SLUG package to investigate the properties of the ionising stellar populations within these HII regions. Finally, we have quantified two pre-SN stellar feedback mechanisms and quantified them as a function of the selected environmental properties. This has allowed us to investigate the evolution of stellar feedback within low-mass, low-metallicity HII regions, and make comparisons to observations of more massive, metal-rich star-forming galaxies from the recently published results of the PHANGS-MUSE survey (Barnes et al. 2021).

The key findings of this paper are summarised as follows:

1. There are considerable discrepancies between the different methods for determining the oxygen abundance using strong-line ratios. To increase our confidence in the oxygen abundance values we have reported, and therefore in our interpretations of the results, deeper spectra of these galaxies covering temperature-sensitive auroral lines for the direct method would be necessary.
2. We estimate that the HII regions within our sample are low-mass ($M_* \lesssim 6 \times 10^4 M_\odot$) and evolved ($T \gtrsim 4.5$ Myr) regions and we therefore believe that their bolometric luminosities are underestimated in most cases if one assumes a fully sampled IMF.
3. We see that stochastic sampling effects can significantly affect the trends observed between feedback-related pressure terms and properties of the HII regions. This stresses the importance of stochastic sampling in the low-mass regime.
4. Our simulated SLUG libraries for Leo P are consistent with a previously reported late O-type star within Leo P's HII region, which we find to be of mass $23^{+4}_{-7} M_\odot$ and age 8^{+2}_{-1} Myr. This illustrates the success of SLUG at identifying massive stars from observations that may not have the necessary spatial resolution for traditional techniques.
5. For all HII regions in our sample, the pressure of the ionised gas is greater than the direct radiation pressure. This supports the findings of feedback studies of other giant HII regions, such as in Olivier et al. (2021) and Barnes et al. (2021). This suggests that photoionisation is more dominant than the direct radiation pressure within these evolved HII regions.
6. The two feedback mechanisms that we have quantified are shown, overall, to decrease with region size, supporting literature findings that these feedback mechanisms have less of an importance in giant, evolved HII regions when compared to ultra-compact HII regions.
7. We find that the direct radiation pressure within HII regions increases with metallicity. In some cases, this may follow from more rapid expansion in metal-poor, and hence hotter regions.
8. Deeper spectra covering the auroral lines necessary for determining the electron temperature and the oxygen abundance via the direct method are required to fully investigate relationships between $P_{...}$ and the ionised gas and stellar properties of HII regions.

In conclusion, we find that an investigation of stellar feedback in the extreme environments of low-metallicity, dwarf starburst galaxies, along with comparisons to more massive systems, can provide a wide range of physical properties to probe the environmental dependence of stellar feedback mechanisms. Follow-up investigations, such as deeper spectroscopic observations, IR and X-ray data, and investigations into the full sample of star-forming galaxies provided by DWALIN and other upcoming surveys, will provide further observational constraints on these mechanisms of stellar feedback and how they affect the evolution of galaxies.

Rowland et al. (2024, arXiv 2402.12497)

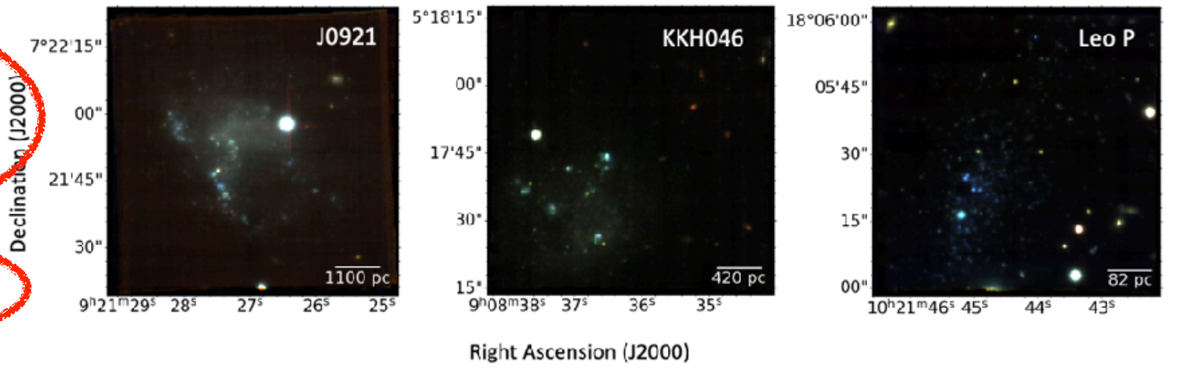

Fig. 1: Three-colour composite images of the three dwarf galaxies (left: J0921, centre: KKH046, right: Leo P) collapsed across three arbitrary wavelength ranges and coloured blue (4650-5800 Å), green (5800-7000 Å) and red (7000-8200 Å).

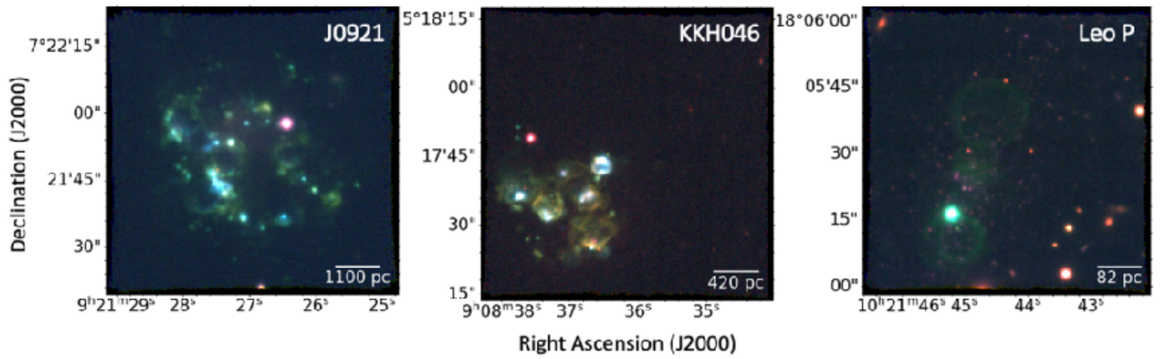

Fig. 2: Same as Figure 1, except here red corresponds to [SII]λ6716, green to Hα and blue to [OIII]λ5007 emission.

Ángel R. López-Sánchez @El_Lobo_Rayado
MACQUARIE University

Evolution of the N/O ratio with the O/H in star-forming galaxies

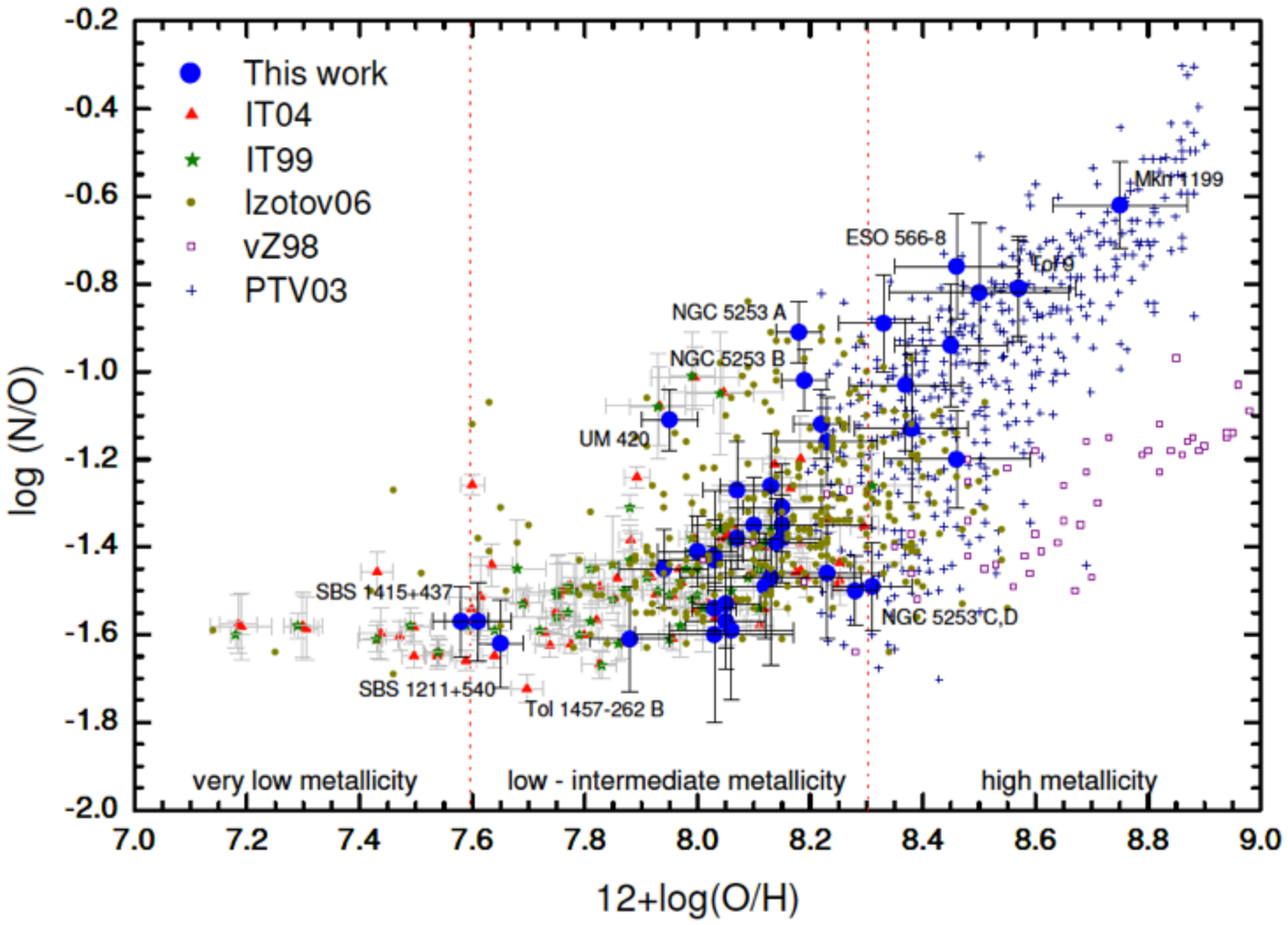

López-Sánchez & Esteban, 2010b, A&A, 517, 85

Kobulnicky et al. 1997; Izotov et al 2006; Pérez-Montero & Contini 2009

Constant for 12+log O/H < 7.6 : *Primary production*

Izotov & Thuan (1999) However see Henry et al. 2000, Pilyugin et al. 2003, Mollá et al. 2006, Berg et al. 2012

Dispersion for 7.6 < 12+log O/H < 8.3 :
Delay in N production & loss via galactic winds
(e.g. Kobulnicky & Skillman 1999)

Increases for 12+log O/H > 8.3:
Metallicity-dependence of N in both massive and intermediate-mass stars
Secondary production (e.g. Pilyugin et al. 2003)

What about chemical abundances that are not O or N?

Galaxy	T_e[a]	12+log(O/H)	log $\frac{O^{++}}{O^+}$	log(N/O)	log(S/O)	log(Ne/O)	log(Ar/O)	log(Fe/O)
HCG 31 AC	D	8.22 ± 0.05	1.51 ± 0.12	−1.12 ± 0.08	...	−0.93 ± 0.12	...	−2.12 ± 0.21
HCG 31 B	D	8.14 ± 0.08	0.63 ± 0.09	−1.39 ± 0.10	−1.67 ± 0.14	−0.42 ± 0.13	...	−1.87 ± 0.32
HCG 31 E	D	8.13 ± 0.09	1.00 ± 0.11	−1.26 ± 0.12	−1.58 ± 0.15	−0.42 ± 0.14	...	−1.77 ± 0.32
HCG 31 F1	D	8.07 ± 0.06	3.72 ± 0.32	−1.27 ± 0.11	−1.69 ± 0.15	−0.80 ± 0.17	...	−1.9:
HCG 31 F2	D	8.03 ± 0.10	2.19 ± 0.21	−1.43 ± 0.16	−1.67 ± 0.18	−0.76 ± 0.20	...	...
HCG 31 G	D	8.15 ± 0.07	1.15 ± 0.11	−1.31 ± 0.10	−1.67 ± 0.22	−0.56 ± 0.14	...	−2.0:
Mkn 1087	EC	8.57 ± 0.10	0.55 ± 0.18	−0.81 ± 0.12	−1.78 ± 0.16	−0.45 ± 0.17	...	...
Mkn 1087 N	EC	8.23 ± 0.10	0.99 ± 0.25	−1.46 ± 0.15	...	−0.52 ± 0.19	...	...
Haro 15 C	EC	8.37 ± 0.10	−0.23 ± 0.16	−1.03 ± 0.15	−1.71 ± 0.18	−0.65 ± 0.18	...	−2.2:
Haro 15 A	D	8.10 ± 0.06	0.66 ± 0.10	−1.35 ± 0.11	−1.89 ± 0.15	−0.68 ± 0.12	...	−1.6:
Mkn 1199	D	8.75 ± 0.12	−0.36 ± 0.16	−0.62 ± 0.10	−1.54 ± 0.14	−0.58 ± 0.17	...	−1.86 ± 0.26
Mkn 1199 NE	EC	8.46 ± 0.13	−0.19 ± 0.09	−1.20 ± 0.11	−1.54 ± 0.17	−0.65 ± 0.18	...	...
Mkn 5	D	8.07 ± 0.04	0.25 ± 0.08	−1.38 ± 0.07	−1.62 ± 0.11	−0.80 ± 0.13	−2.31 ± 0.12	−1.96 ± 0.18
IRAS 08208+2816	D	8.33 ± 0.08	0.43 ± 0.12	−0.89 ± 0.11	−1.64 ± 0.16	−0.67 ± 0.13	−2.51 ± 0.15	−1.95 ± 0.17
IRAS 08339+6517	EC	8.45 ± 0.10	0.53 ± 0.16	−0.94 ± 0.14	...	−0.45 ± 0.18	...	...
IRAS 08339+6517c	EC	8.38 ± 0.10	0.81 ± 0.21	−1.13 ± 0.17	...	−0.55:	...	...
POX 4	D	8.03 ± 0.04	0.74 ± 0.06	−1.54 ± 0.06	−1.80 ± 0.10	−0.78 ± 0.10	...	−2.17 ± 0.11
POX 4c	EC	8.03 ± 0.14	−0.30 ± 0.22	−1.60 ± 0.20	...	-0.60:	...	...
UM 420	D	7.95 ± 0.05	0.00 ± 0.08	−1.11 ± 0.07	−1.66 ± 0.13	−0.71 ± 0.13	...	−2.16 ± 0.13
SBS 0926+606 A	D	7.94 ± 0.08	0.42 ± 0.12	−1.45 ± 0.09	−1.60 ± 0.13	...	−2.34 ± 0.13	−1.99 ± 0.16
SBS 0926+606 B	EC	8.15 ± 0.16	0.21 ± 0.14	−1.35 ± 0.12	...	...	...	...
SBS 0948+532	D	8.03 ± 0.05	0.61 ± 0.08	−1.42 ± 0.08	−1.69 ± 0.14	−0.73 ± 0.12	...	−1.78 ± 0.10
SBS 1054+365	D	8.00 ± 0.07	0.70 ± 0.11	−1.41 ± 0.08	−1.79 ± 0.15	−0.67 ± 0.11	−2.29 ± 0.14	...
SBS 1054+365 b	EC	8.13 ± 0.16	−0.35 ± 0.20	−1.47 ± 0.20	...	...	...	...
SBS 1211+540	D	7.65 ± 0.04	0.69 ± 0.07	−1.62 ± 0.10	−1.47 ± 0.14	−0.75 ± 0.10	...	...
SBS 1319+579 A	D	8.05 ± 0.06	0.77 ± 0.12	−1.53 ± 0.10	−1.76 ± 0.10	...	−2.41 ± 0.11	...
SBS 1319+579 B	D	8.12 ± 0.10	0.16 ± 0.19	−1.49 ± 0.12	−1.76 ± 0.14	...	...	...
SBS 1319+579 C	D	8.15 ± 0.07	0.18 ± 0.13	−1.38 ± 0.10	−1.60 ± 0.11	...	...	−2.3:
SBS 1415+437 C	D	7.58 ± 0.05	0.35 ± 0.08	−1.57 ± 0.08	−1.62 ± 0.12	...	−2.31 ± 0.13	−1.91 ± 0.13
SBS 1415+437 A	D	7.61 ± 0.06	0.42 ± 0.14	−1.57 ± 0.09	−1.72 ± 0.14	...	...	−1.9:
III Zw 107 A	D	8.23 ± 0.09	0.12 ± 0.14	−1.16 ± 0.10	−1.82 ± 0.15	−0.73 ± 0.15	−2.46 ± 0.13	−2.3:
Tol 9	D	8.57 ± 0.10	0.16 ± 0.17	−0.81 ± 0.11	−1.62 ± 0.12	−0.72 ± 0.14	−2.55 ± 0.15	−2.1:
Tol 1457-262 A	D	8.05 ± 0.07	0.27 ± 0.11	−1.57 ± 0.11	−1.88 ± 0.13	−0.88 ± 0.18	−2.50 ± 0.13	−2.2:
Tol 1457-262 B	D	7.88 ± 0.07	0.43 ± 0.11	−1.61 ± 0.12	−1.72 ± 0.18	−0.88 ± 0.20	−2.44 ± 0.18	−1.90 ± 0.22
Tol 1457-262 C	D	8.06 ± 0.11	0.14 ± 0.16	−1.59 ± 0.16	...	−0.84 ± 0.22	−2.45 ± 0.20	...
ESO 566-8	D	8.46 ± 0.11	−0.19 ± 0.17	−0.76 ± 0.12	...	−0.56 ± 0.19	−2.17 ± 0.19	−2.5:
ESO 566-7	EC	8.50 ± 0.16	−0.57 ± 0.22	−0.82 ± 0.16	...	...	−2.49 ± 0.25	...
NGC 5253 A	D	8.18 ± 0.04	2.88 ± 0.18	−0.91 ± 0.07	−1.58 ± 0.08	−0.71 ± 0.08	−2.19 ± 0.07	−2.10 ± 0.12
NGC 5253 B	D	8.19 ± 0.04	3.09 ± 0.14	−1.02 ± 0.07	−1.60 ± 0.08	−0.70 ± 0.08	−2.21 ± 0.07	−2.18 ± 0.11
NGC 5253 C	D	8.28 ± 0.04	1.95 ± 0.13	−1.50 ± 0.08	−1.69 ± 0.09	−0.74 ± 0.08	−2.30 ± 0.08	−2.46 ± 0.14
NGC 5253 D	D	8.31 ± 0.07	0.56 ± 0.14	−1.49 ± 0.10	−1.74 ± 0.13	−0.70 ± 0.15	−2.30 ± 0.13	−2.25 ± 0.16

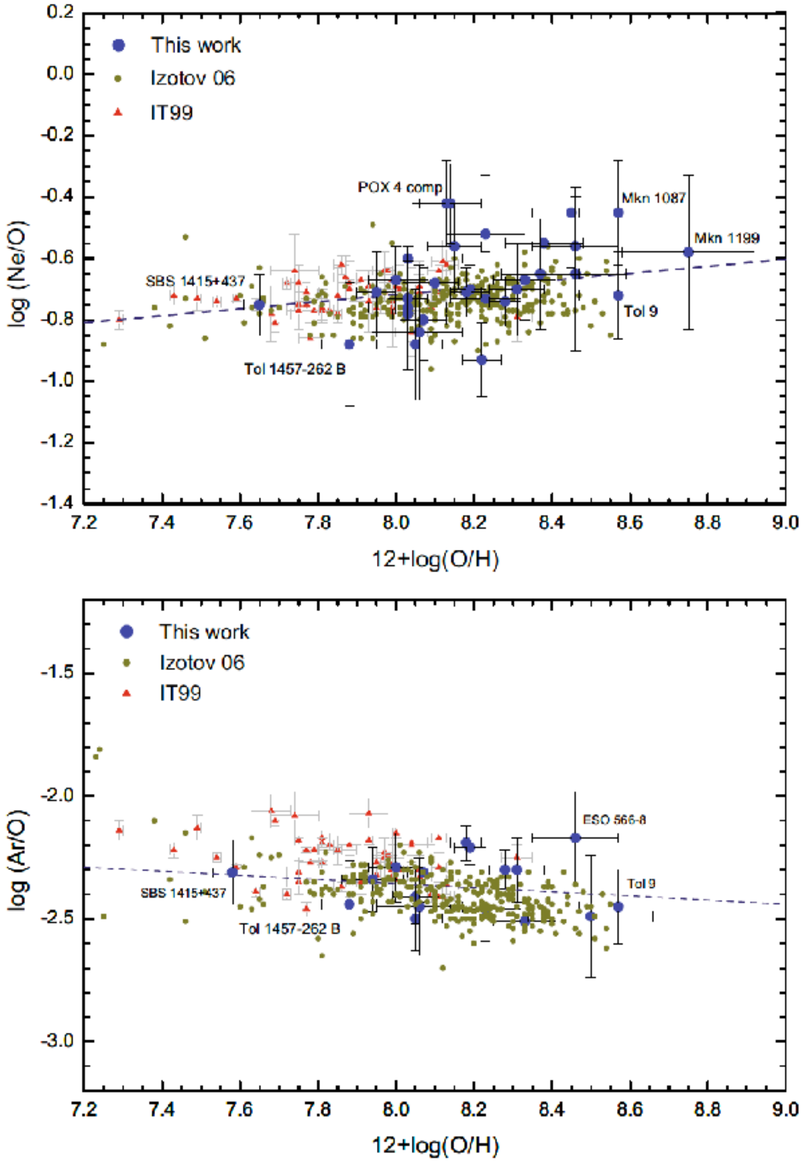

López-Sánchez & Esteban 2010b

Evolution of the N/O ratio with the O/H in star-forming galaxies

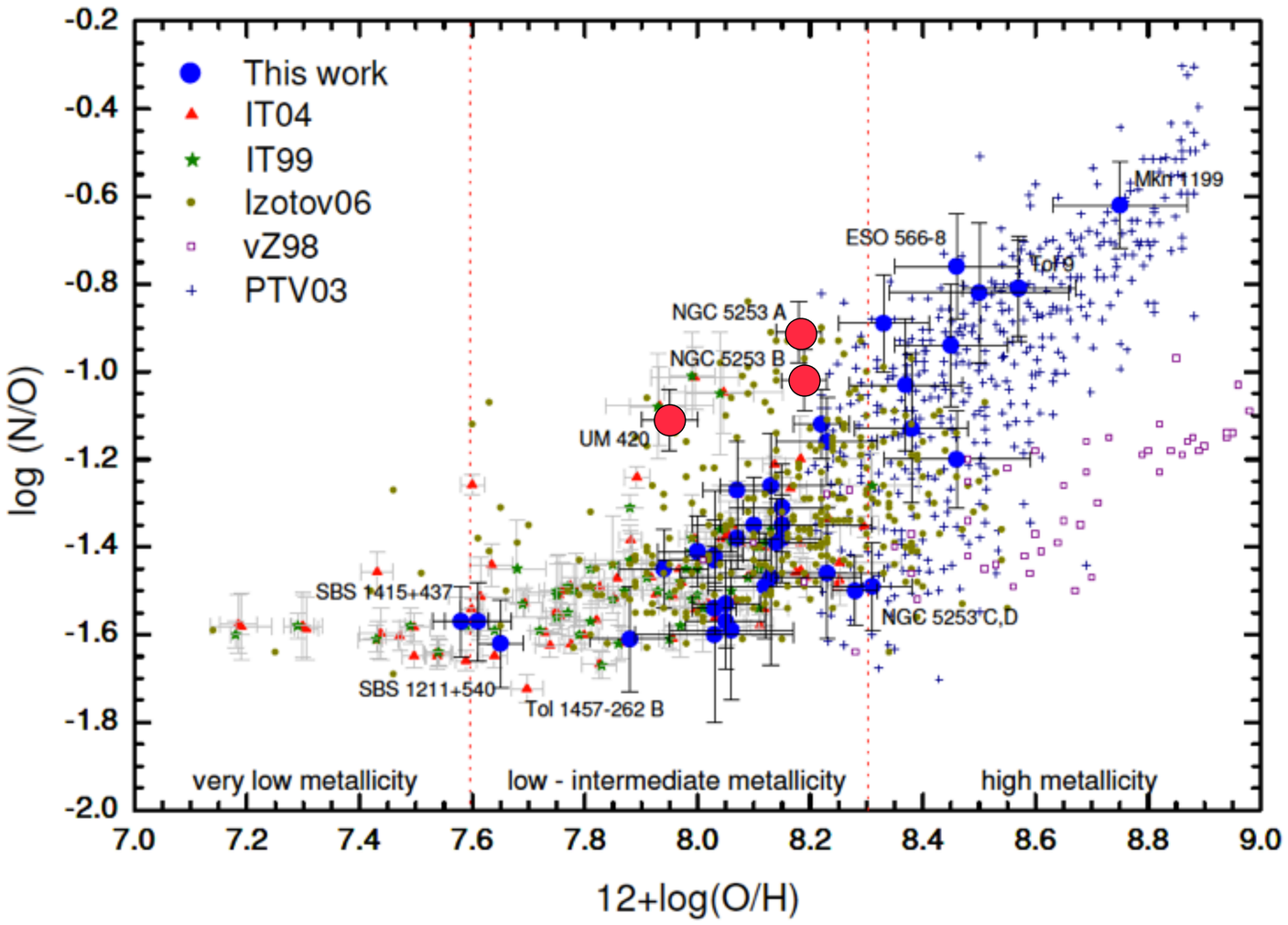

López-Sánchez & Esteban, 2010b, A&A, 517, 85

Kobulnicky et al. 1997; Izotov et al 2006; Pérez-Montero & Contini 2009

Constant for 12+log O/H < 7.6 : *Primary production*

Izotov & Thuan (1999) However see Henry et al. 2000, Pilyugin et al. 2003, Mollá et al. 2006, Berg et al. 2012

Dispersion for 7.6 < 12+log O/H < 8.3 :
Delay in N production & loss via galactic winds
(e.g. Kobulnicky & Skillman 1999)

Increases for 12+log O/H > 8.3:
Metallicity-dependence of N in both massive and intermediate-mass stars
Secondary production (e.g. Pilyugin et al. 2003)

Some objects with very high N/O ratio. Chemical pollution by winds of WR stars?

Important to consider Star Formation Histories, in agreement with predictions by theoretical models (e.g., Mollá et al. 2006)

Ángel R. López-Sánchez @El_Lobo_Rayado

NGC 4861 with PMAS: SFH + SFR, WR

Roche et al. (2023)

ABSTRACT

Using the PMAS Integral Field Unit on the Calar Alto 3.5 m telescope, we observed the southern component (Markarian 59) of the 'cometary' starburst galaxy NGC 4861. Mrk 59 is centred on a giant nebula and concentration of stars 1 kpc in diameter. Strong Hα emission points to a star-formation rate (SFR) at least 0.47 $M_\odot$ yr^{-1}. Mrk 59 has a very high [O III] λ5007/Hβ ratio, reaching 7.35 in the central nebula, with a second peak at a star-forming hotspot further north. Fast outflows are not detected but nebular motion and galaxy rotation produce relative velocities up to 40 km s^{-1}. Spectral analysis of different regions with 'Fitting Analysis using Differential evolution Optimization' (FADO) finds that the stars in the central and 'spur' nebulae are very young, $\leq$ 125 Myr with a large $<$ 10 Myr contribution. Older stars ($\sim$ 1 Gyr) make up the northern disk component, while the other regions show mixtures of 1 Gyr age with very young stars. This and the high specific SFR $\sim$ 3.5 Gyr^{-1} imply a bimodal star formation history, with Mrk 59 formed in ongoing starbursts fuelled by a huge gas inflow, turning the galaxy into an asymmetric 'green pea' or blue compact dwarf. We map the He II λ4686 emission, and identify a broad component from the central nebula, consistent with the emission of $\sim$300 Wolf–Rayet stars. About a third of the He II λ4686 flux is a narrow line emitted from a more extended area covering the central and spur nebulae, and may have a different origin.

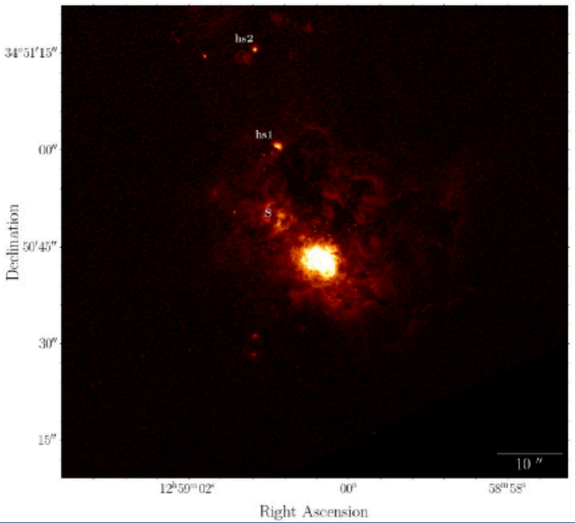

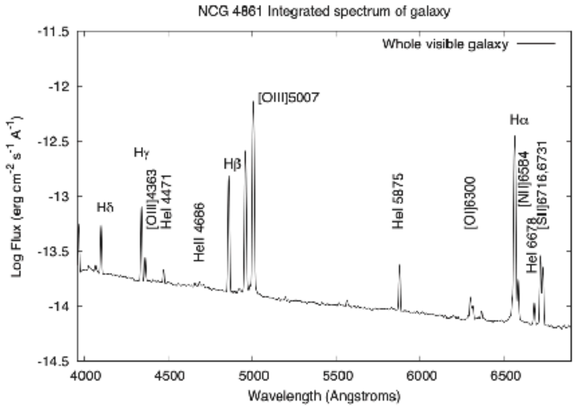

Figure 4. PMAS spectrum integrated over the whole visible galaxy (the 2114 spaxels with Hα flux above a threshold 10^{-16} erg cm^{-2}s^{-1}) in log scale.

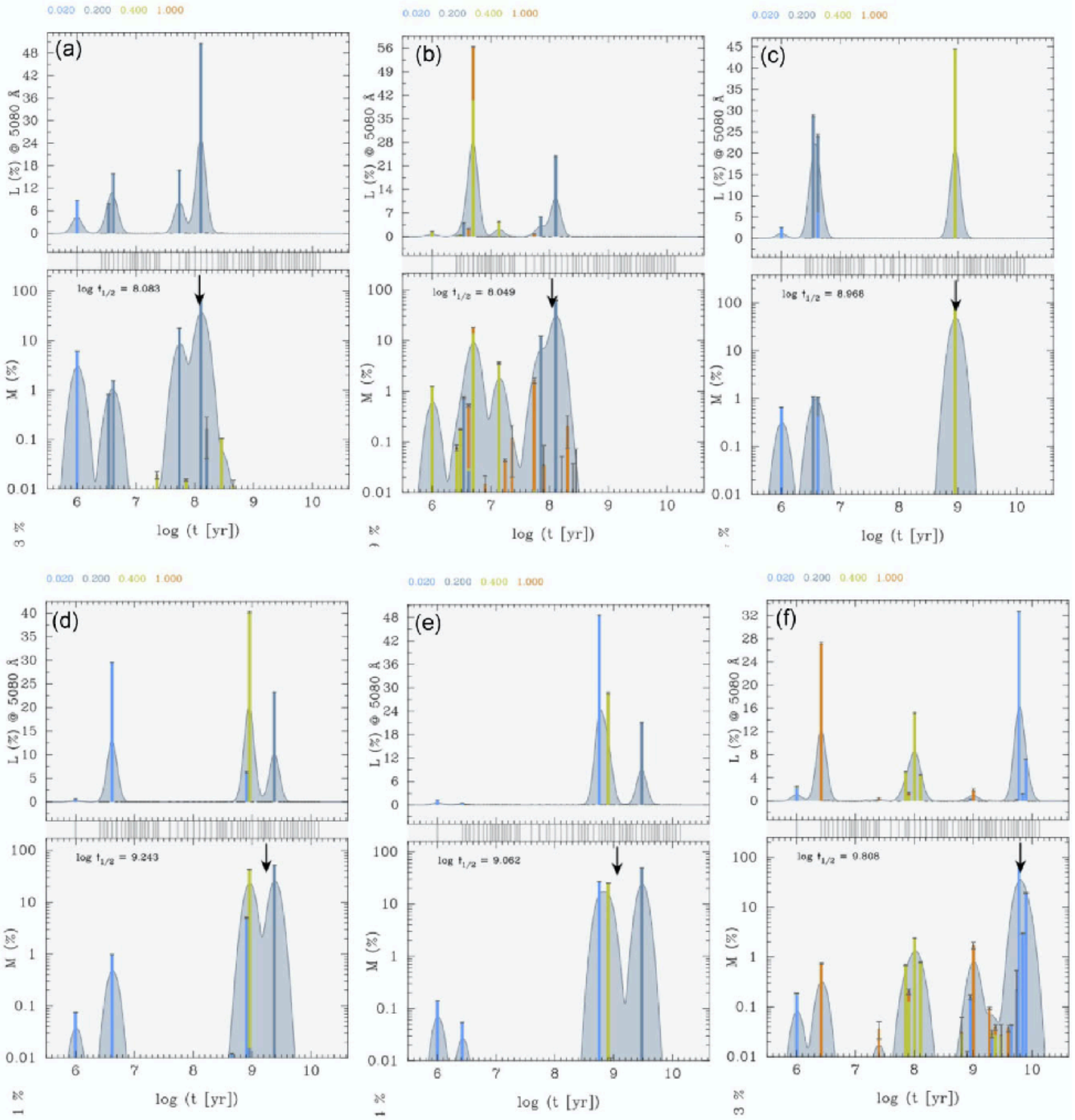

ESO 338-IG04 with MUSE: WR & SF feedback, chemical pollution, escaping of LyC photons

7. Summary and conclusions

We presented deep VLT/MUSE optical integral field observations of the blue compact galaxy ESO 338-IG04. Based on analysis of the emission line spectra as well as HST observations of the cluster population we derived the following results:

1. ESO 338 is surrounded by an extended ionized halo, which we can trace to 9 kpc distance from the centre. We derived a total mass of the ionized gas of $3.0 \times 10^7\,M_\odot$, by extrapolating the measured radial density profile as far out as the measured Hα SB profile.
2. We identified four clusters showing the blue and/or red WR bump in their spectra. Re-fitting the observed SEDs of the clusters obtained from HST imaging data reveal that these clusters have masses above $10^5\,M_\odot$ and ages between 3 and 6 Myr, consistent with the observed WR features.
3. The ionization maps reveal the ionization channels detected earlier, but extending out even further to the north and the south to the edges of the observed halo. Additionally we found an increase with ionization when going to larger radii, suggesting that the halo of ESO 338 is density bounded. Diffuse He II is found in the highly ionized central regions of the galaxy, consistent with ionization by WR and O stars.
4. The kinematical information derived from the Hα line reveals a complex velocity structure of the halo. Similar to previous studies, no rotational motion could be identified in ESO 338. Instead the galaxy is a highly dispersion dominated galaxy with a $v_{\rm shear}/\sigma_0 = 0.5$, similar to what is seen in high redshift star forming galaxies.
5. A spatially resolved analysis of the BPT diagram revealed that the gas in the central starburst as well as the inner ~kpc of the outflows are dominated by photoionization. Towards one of the WR clusters we observed a very high [O III]/Hβ ratio, indicative of the WR stars ionizing the surrounding gas to extreme levels. Outside the central regions, shocks start to become important. We found a ring of shocked gas around the central starburst. We interpreted this as an expanding super bubble filled with hot gas created by the stellar wind and supernova feedback.
6. We found areas in the ISM with enriched nitrogen. This is consistent with the enrichment by WR stars. The regions with strong enrichment have an elongated spatial extend and show a velocity pattern different from that of the bulk of the gas detected in Hα. Towards the base of the features two stellar clusters are identified with ages slightly older than that of WR clusters. These clusters have formed their own small bubble with hot gas of which the nitrogen enriched gas is flowing out in a different direction than the bulk of the gas in the galaxy.
7. The Hα kinematics reveals complex outflows towards the north and the south of the galaxy. Both outflows show a complex spatial as well as spectral structure, suggesting that multiple clusters are responsible for this. We found shocks at the end of the galactic outflows. This can be interpreted as hot outflowing gas colliding with the more quiescent warm ISM or by high density gas becoming kinematically unstable when entering low density gas. The turbulence created by these instabilities would then be responsible for the observed shocks.
8. The ISM and halo of ESO 338 is highly modified by the stellar feedback of the massive star clusters in ESO 338. All feedback mechanisms act and become important in different areas and on different timescales. The mechanical feedback of the stars and supernovae is responsible for the shocks and outflows, modifying the spatial distribution of the ionized gas. Photoionization by the WR and O stars sets the ionzization structure of the halo and results in a density bounded halo, facilitating the escape of LyC photons. Finally the ISM is chemically enriched by the WR winds.

Bik et al. (2018)

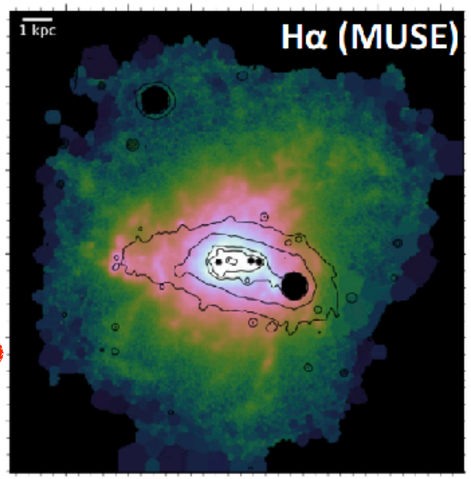

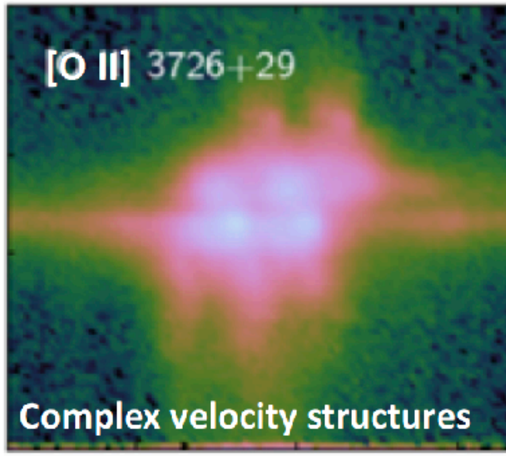

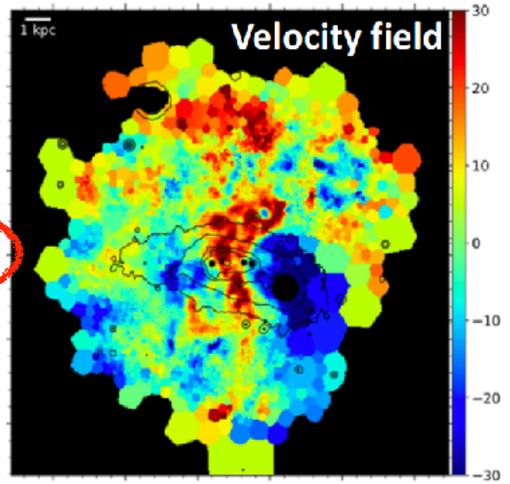

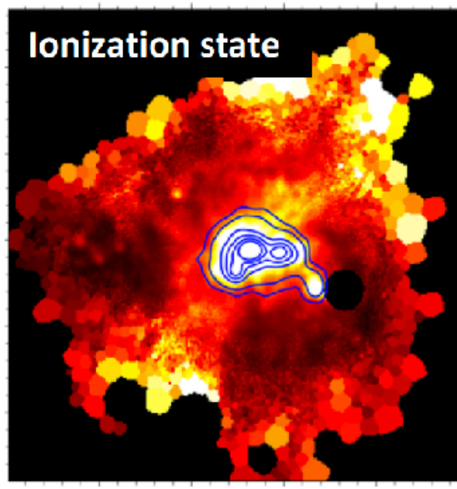

Ángel R. López-Sánchez @El_Lobo_Rayado

Haro 11 with MUSE: T_e & abundance discrepancies, complex kinematics, feedback…

We use high quality VLT/MUSE data to study the kinematics and the ionized gas properties of Haro 11, a well-known starburst merger system and the closest confirmed Lyman continuum leaking galaxy. We present results from integrated line maps, and from maps in three velocity bins comprising the blueshifted, systemic, and redshifted emission. The kinematic analysis reveals complex velocities resulting from the interplay of virial motions and momentum feedback. Star formation happens intensively in three compact knots (knots A, B, and C), but one, knot C, dominates the energy released in supernovae. The halo is characterized by low gas density and extinction, but with large temperature variations, coincident with fast shock regions. Moreover, we find large temperature discrepancies in knot C, when using different temperature-sensitive lines. The relative impact of the knots in the metal enrichment differs. While knot B is strongly enriching its closest surrounding, knot C is likely the main distributor of metals in the halo. In knot A, part of the metal enriched gas seems to escape through low density channels towards the south. We compare the metallicities from two methods and find large discrepancies in knot C, a shocked area, and the highly ionized zones, that we partially attribute to the effect of shocks. This work shows, that traditional relations developed from averaged measurements or simplified methods, fail to probe the diverse conditions of the gas in extreme environments. We need robust relations that include realistic models where several physical processes are simultaneously at work.

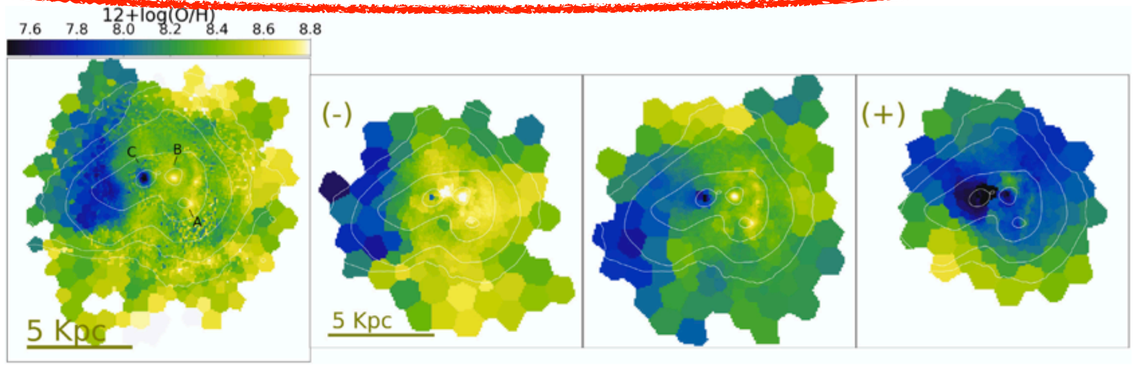

Figure 9. Oxygen metallicities derived from the direct method. The top panel shows the integrated metallicities while the three smaller panels in the second row display the metallicities of the blueshifted (-), central (c), and redshifted (+) gas.

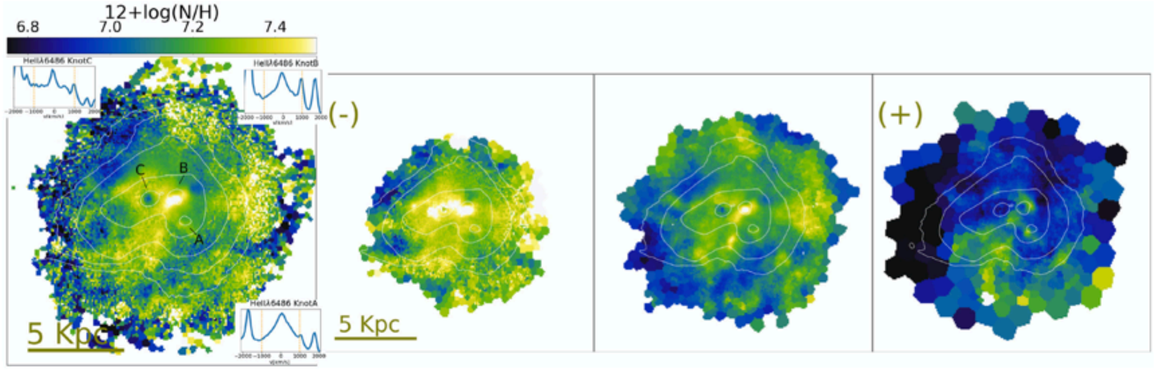

Figure 10. Nitrogen metallicities derived from the direct method. The top panel shows the integrated metallicities while the three smaller panels in the second row display the metallicities of the blueshifted (-), central (c), and redshifted (+) gas. For the three knots we show insets of the He IIλ4686 spectral line, which is an indicator of the strong WR winds.

- LyC leaking galaxy (Bergvall et al. 2006, Leitet et al. 2011)
- Menacho et al. (2019, 2021)

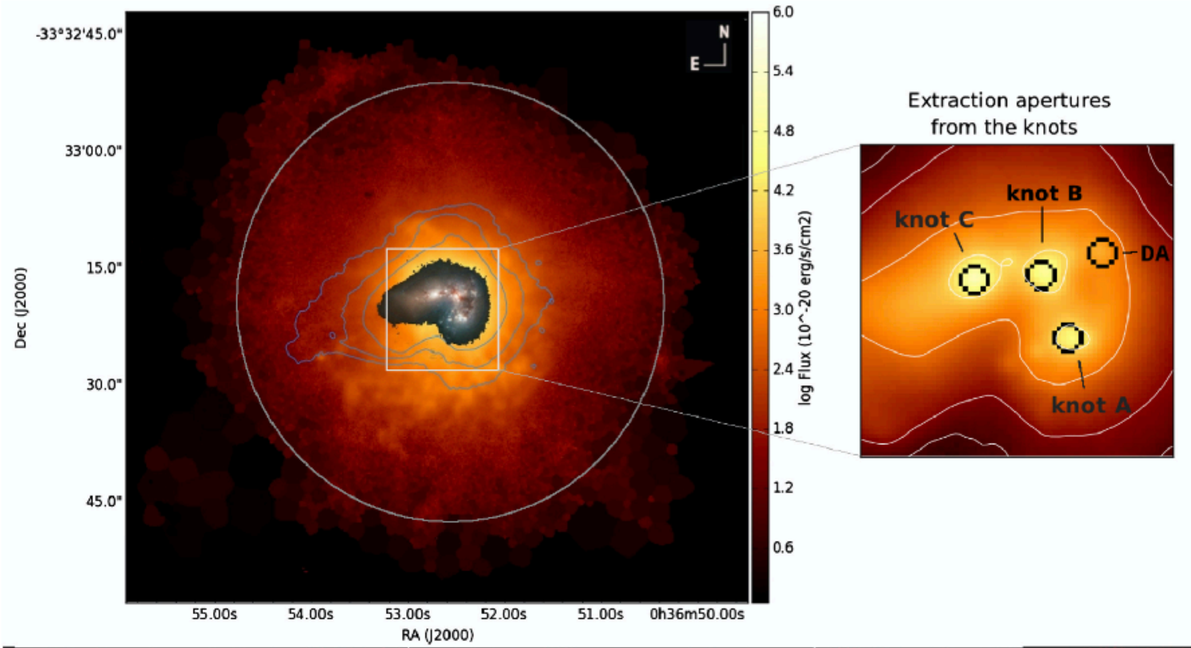

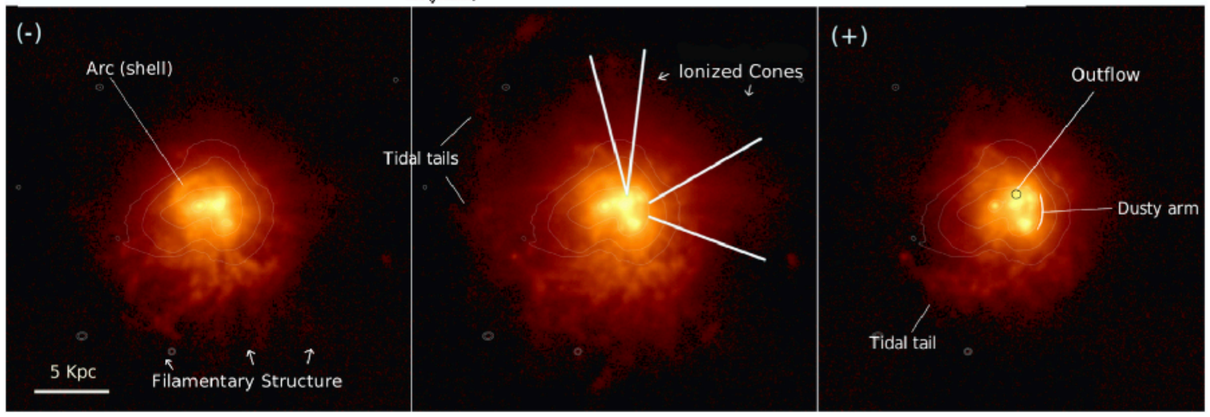

Mrk 1486: asymmetric metal-rich outflows & metal-poor inflows

- DUVET survey, Cameron et al. 2021 using Keck/Keck Cosmic Web Imager (KCWI) observations along both the major and minor axes.

"Metal-enriched outflows and metal-poor inflows are frequently invoked as important mechanisms for explaining a number of galaxy observables including scaling relations. The difference between our $Z_{outflow}/Z_{ISM}$ and those derived by Chisholm et al. (2018) are a factor 2-3, adding its asymmetry are both reasons emphasizing the dire need for observations like those reported here to understand basic observables"

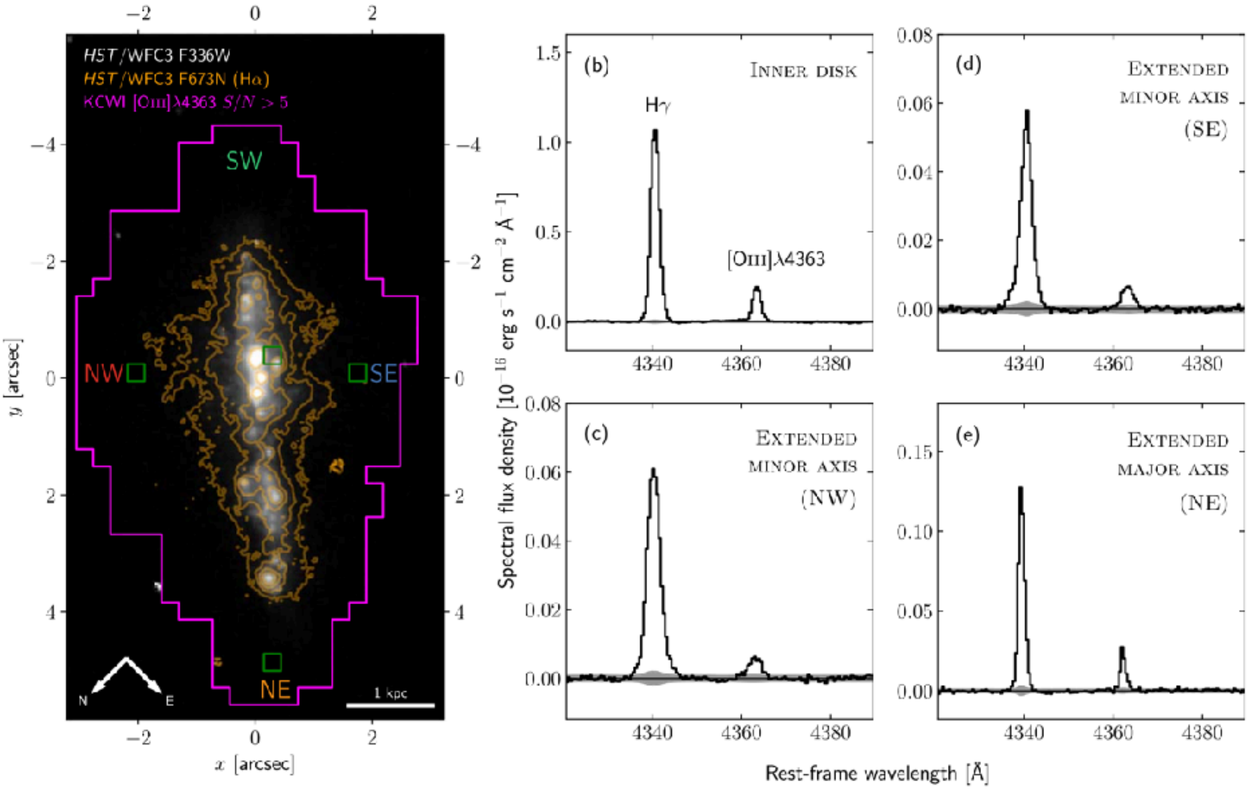

We present electron temperature (T_e) maps for the edge-on system Mrk 1486, affording "direct-method" gas-phase metallicity measurements across 5″.8 (4.1 kpc) along the minor axis and 9″.9 (6.9 kpc) along the major axis. These maps, enabled by strong detections of the [O III] λ4363 auroral emission line across a large spatial extent of Mrk 1486, reveal a clear negative minor-axis T_e gradient in which temperature decreases with increasing distance from the disk plane. We find that the lowest metallicity spaxels lie near the extremes of the major axis, while the highest metallicity spaxels lie at large spatial offsets along the minor axis. This is consistent with a picture in which low-metallicity inflows dilute the metallicity at the edges of the major axis of the disk, while star formation drives metal-enriched outflows along the minor axis. We find that the outflow metallicity in Mrk 1486 is 0.20 dex (1.6 times) higher than the average interstellar medium (ISM) metallicity, and more than 0.80 dex (6.3 times) higher than metal-poor inflowing gas, which we observe to be below 5% $Z_\odot$. This is the first example of metallicity measurements made simultaneously for inflowing, outflowing, and inner disk ISM gas using consistent T_e-based methodology. These measurements provide unique insight into how baryon-cycle processes contribute to the assembly of a galaxy like Mrk 1486.

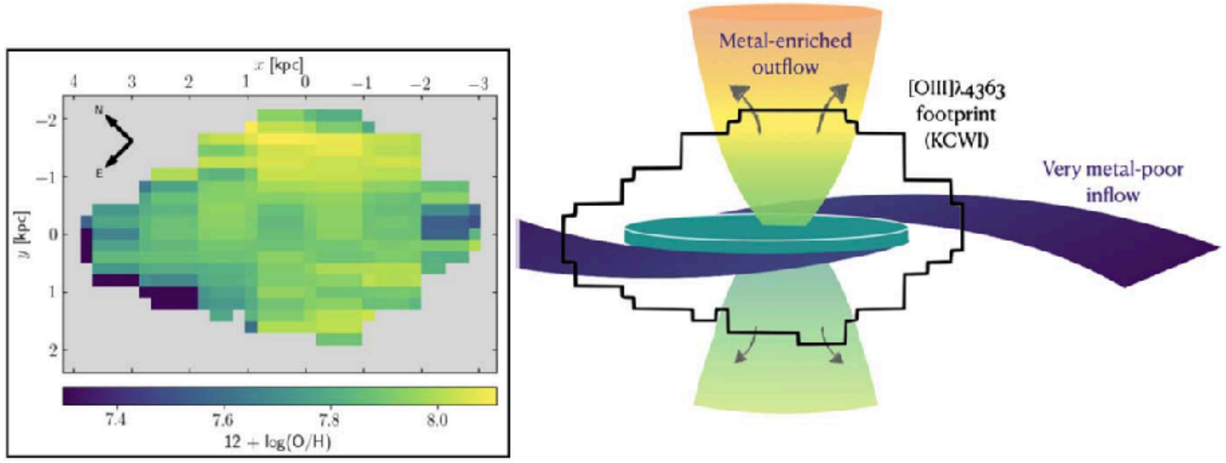

Figure 4. Left: map of inferred metallicities (see Section 4.2). The highest metallicity regions are offset from the disk along the minor axis. The lowest metallicity points are generally at large separations along the major axis. Right: schematic diagram depicting qualitative metallicity differences from different gas flow components. The black footprint shows the extent of the metallicity map from KCWI observations. Our high-metallicity points along the minor axis can be explained by the presence of outflow cones driving out metal-enriched gas. The asymmetry observed along the minor axis may indicate that these outflows are inhomogeneous. Our lowest metallicity points at the extremes of the major axis extend beyond the 90% *i*-band flux radius of Mrk 1486 and consequently may see a much larger dilution effect from the inflow of metal-poor gas. Given we measure metallicity as low as $12 + \log(O/H) \approx 7.3$ (upper limit; refer to Section 4.2) at these extremes, we infer that the source of the inflowing gas may be extremely metal poor.

Ángel R. López-Sánchez @El_Lobo_Rayado

NGC 1569: direct metallicity measurement of outflow (all ~ same O/H)

DUVET survey, Hamel-Bravo et al. (2024, MNRAS, just accepted)

ABSTRACT

We present the results of direct-method metallicity measurements in the disk and outflow of the low-metallicity starburst galaxy NGC 1569. We use Keck Cosmic Web Imager observations to map the galaxy across 54″ (800 pc) along the major axis and 48″ (700 pc) along the minor axis with a spatial resolution of 1″ (~15 pc). We detect common strong emission lines ([O III] λ5007, Hβ, [O II] λ3727) and the fainter [O III] λ4363 auroral line, which allows us to measure electron temperature (T_e) and metallicity. Theory suggests that outflows drive metals out of the disk driving observed trends between stellar mass and gas-phase metallicity. Our main result is that the metallicity in the outflow is similar to that of the disk, $Z_{out}/Z_{ISM} \approx 1$. This is consistent with previous absorption line studies in higher mass galaxies. Assumption of a mass-loading factor of $\dot{M}_{out}/SFR \sim 3$ makes the metal-loading of NGC 1569 consistent with expectations derived from the mass-metallicity relationship. Our high spatial resolution metallicity maps reveal a region around a supermassive star cluster (SSC-B) with distinctly higher metallicity and higher electron density, compared to the disk. Given the known properties of SSC-B the higher metallicity and density of this region are likely the result of star formation-driven feedback acting on the local scale. Overall, our results are consistent with the picture in which metal-enriched winds pollute the circumgalactic medium surrounding galaxies, and thus connect the small-scale feedback processes to large-scale properties of galaxy halos.

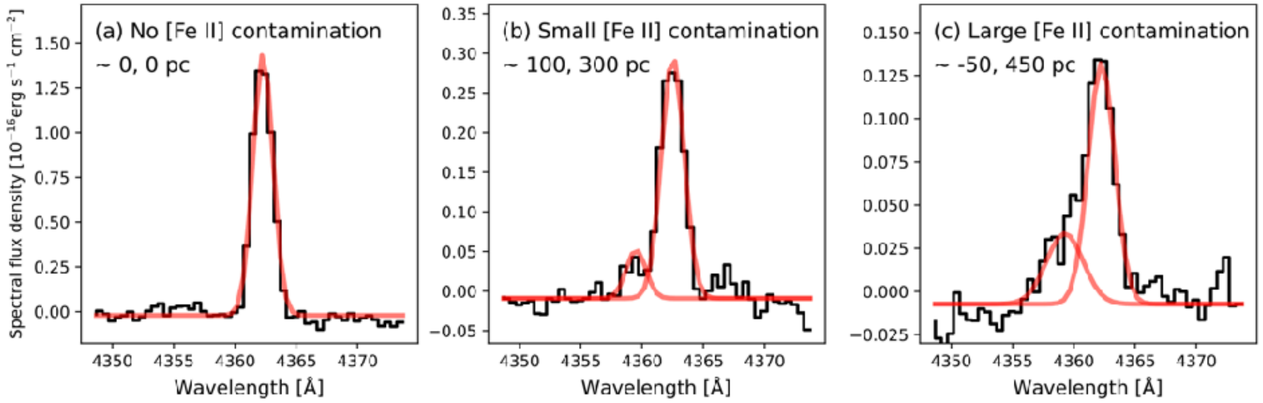

Figure 2. Top row: On the left, emission line flux map of Hβ from KCWI. The x and y-axes show the position to the galaxy center, determined from *Spitzer*/IRAC 3.6μm band observations. We mark the center with a black + symbol. We masked out a 4″ × 4″ region around a foreground star at (0, 700 pc). On the right, the emission line flux map of the [O III] λ4363 line. The spaxel size is 0.87″× 0.87″(13 × 13 pc). SSC B is located near the emission line cavity at (0,200 pc) in the images. Bottom row: three examples of the [O III] λ4363 emission line. Panel (a) shows a spaxel where we observe no [Fe II] λ4360 contamination, panel (b) shows a spaxel with small [Fe II] contamination and panel (c) shows a spaxel with large [Fe II] contamination. The position in the map for each example is indicated in the top right of each panel. In black we show the data and in red the fit using a ΔBIC of 20.

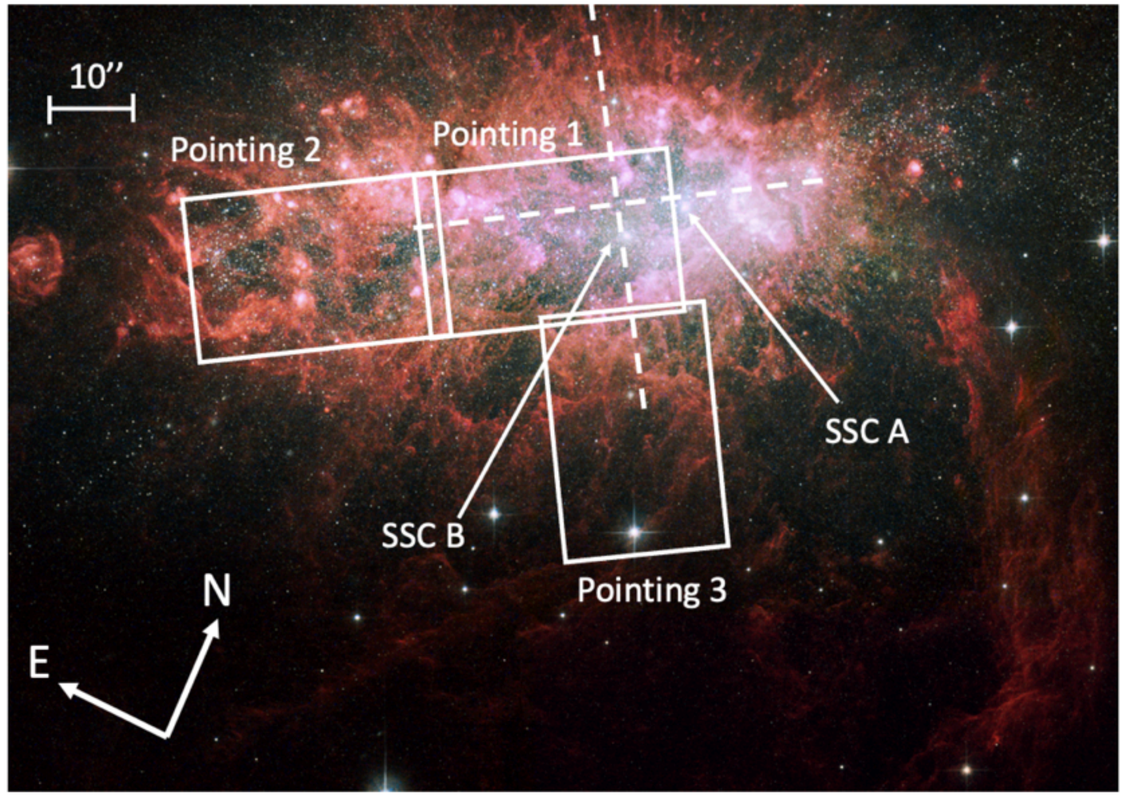

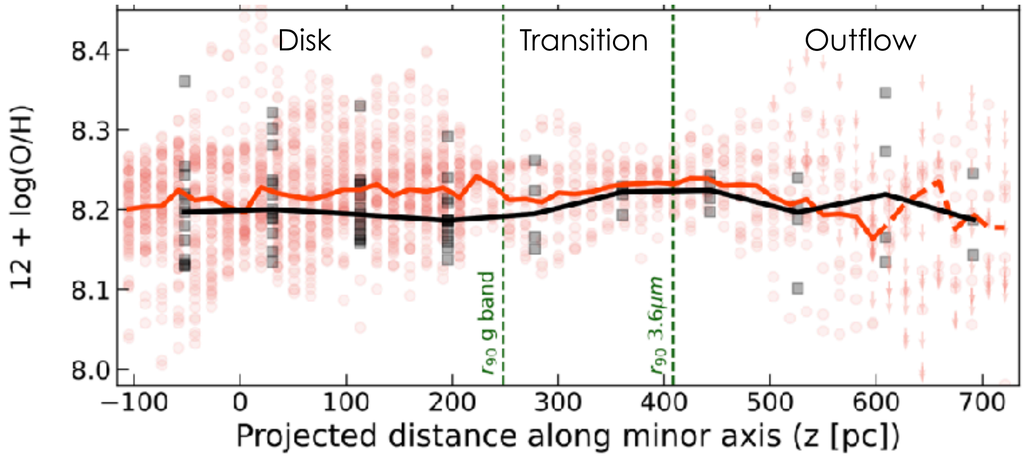

Shaken, but not expelled: Gentle baryonic feedback from nearby starburst dwarf galaxies

Marasco et al. 2023

β = mass-loading factor

Baryonic feedback is expected to play a key role in regulating the star formation of low-mass galaxies by producing galaxy-scale winds associated with mass-loading factors of $\beta \sim 1-50$. We test this prediction using a sample of 19 nearby systems with stellar masses of $10^7 < M_\star/M_\odot < 10^{10}$, mostly lying above the main sequence of star-forming galaxies. We used MUSE at VLT optical integral field spectroscopy to study the warm ionised gas kinematics of these galaxies via a detailed modelling of their Hα emission line. The ionised gas is characterised by irregular velocity fields indicating the presence of non-circular motions of a few tens of km s^{-1} within galaxy discs, but with intrinsic velocity dispersion of 40–60 km s^{-1} that are only marginally larger than those measured in main-sequence galaxies. Galactic winds, defined as gas at velocities larger than the galaxy escape speed, encompass only a few percent of the observed fluxes. Mass outflow rates and loading factors are strongly dependent on $M_\star$, the star formation rate (SFR), SFR surface density, and specific SFR (sSFR). For $M_\star$ of $10^8\,M_\odot$ we find $\beta \simeq 0.02$, which is more than two orders of magnitude smaller than the values predicted by theoretical models of galaxy evolution. In our galaxy sample, baryonic feedback stimulates a gentle gas cycle rather than causing a large-scale blow-out.

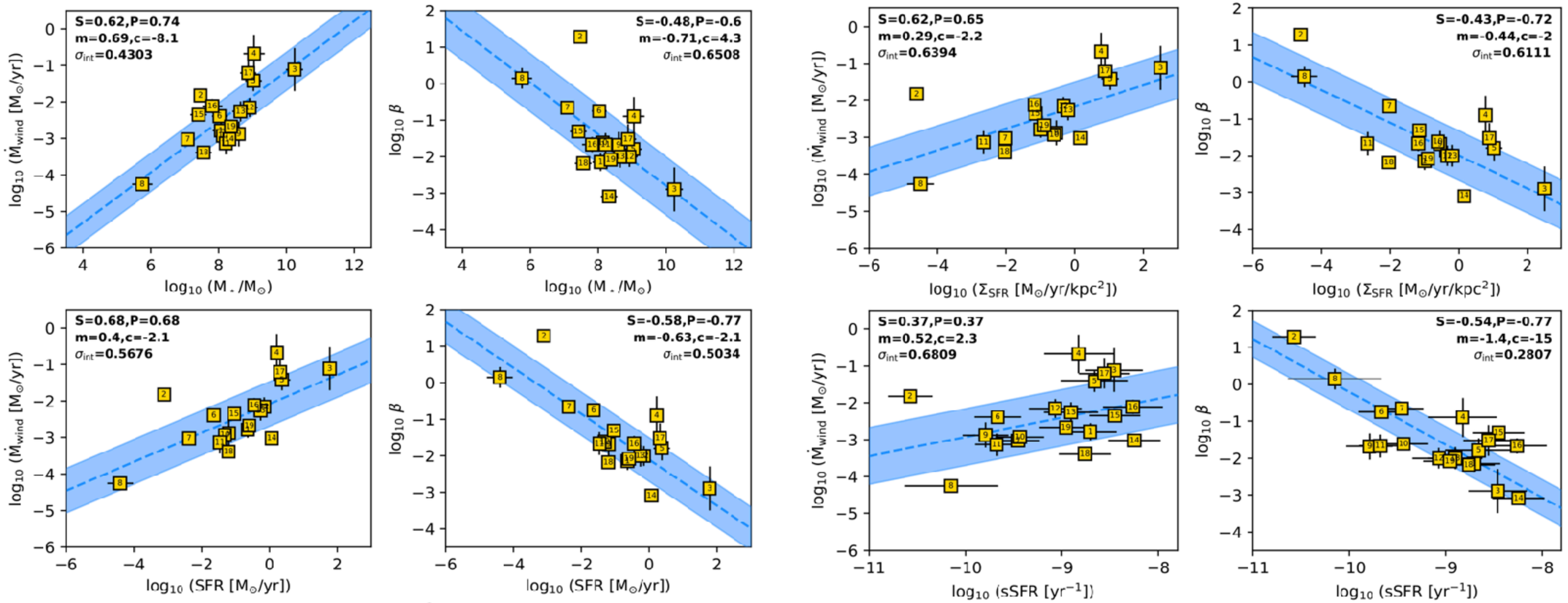

Ángel R. López-Sánchez @El_Lobo_Rayado

Targeting dwarf gas-rich nearby galaxies with KOALA

HI KOALA IFS Dwarf galaxies Survey

Hi-KIDS

https://hikids.datacentral.org.au *PI: Ángel López-Sánchez*

- Exploring a parameter space not studied by current IFS surveys we are obtaining **high-quality IFS data** of **nearby dwarf galaxies** with available **21-cm HI interferometric radio** data.

- We are using **KOALA+AAOmega at the 3.9m AAT** to assemble deep, good-quality IFS data:
  - ✓ 7 x 30 min exposures / pointing
  - ✓ **3650 – 9100 λλ** range:
  - ✓ **[O II] 3727 -> [S III] 9065**.

- Sample selection:
  - ✓ **Local Volume HI Survey**, Koribalski et al. (2018).
  - ✓ **Faint Irregular Galaxy GMRT Survey,** Begum et al. (2008).
  - ✓ **BCDGs observed at the ATCA**, López-Sánchez et al. (2008).

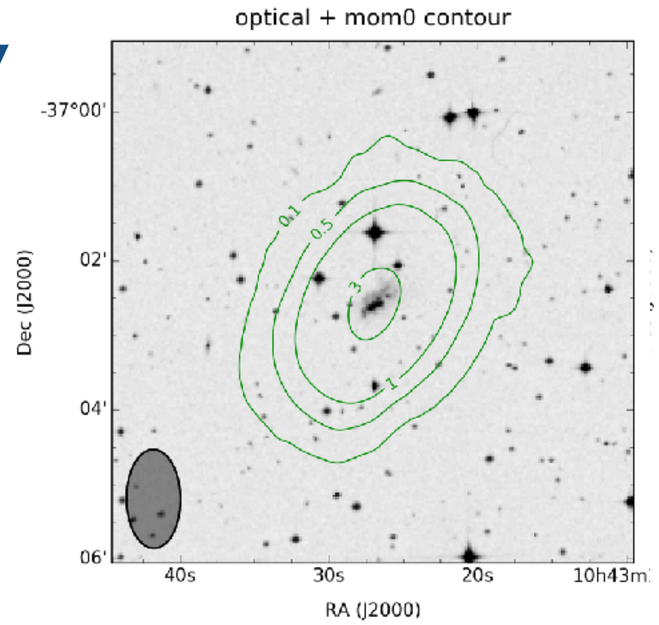

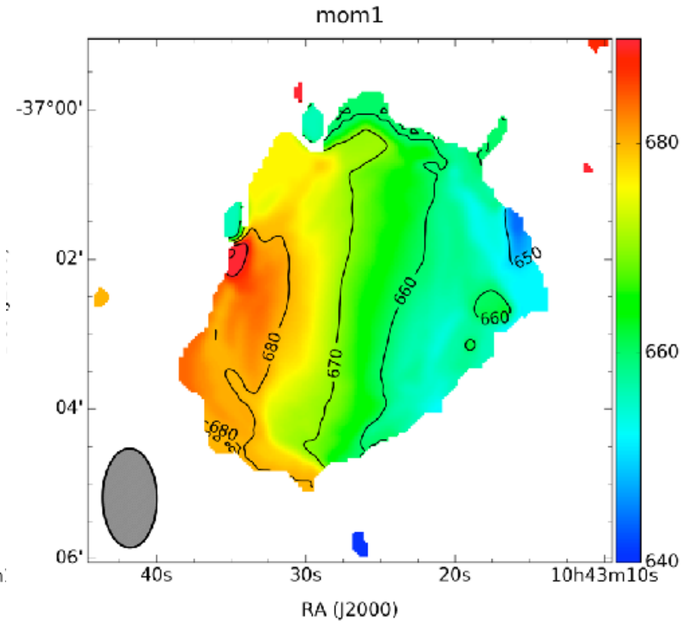

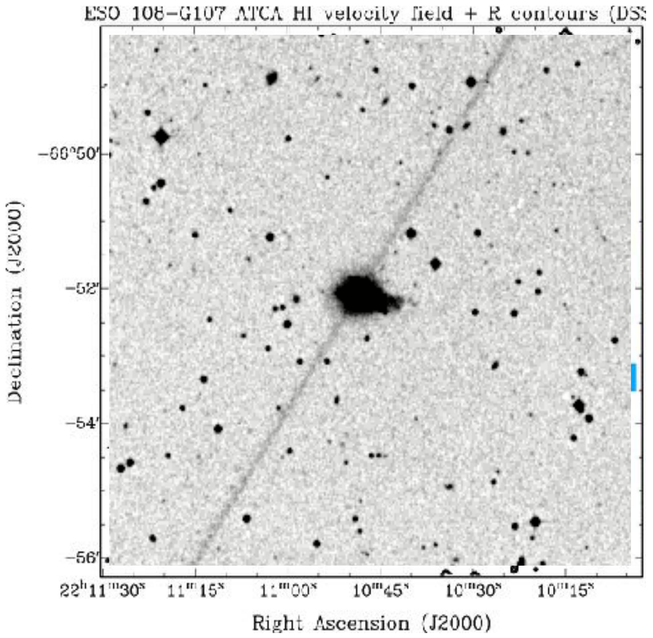

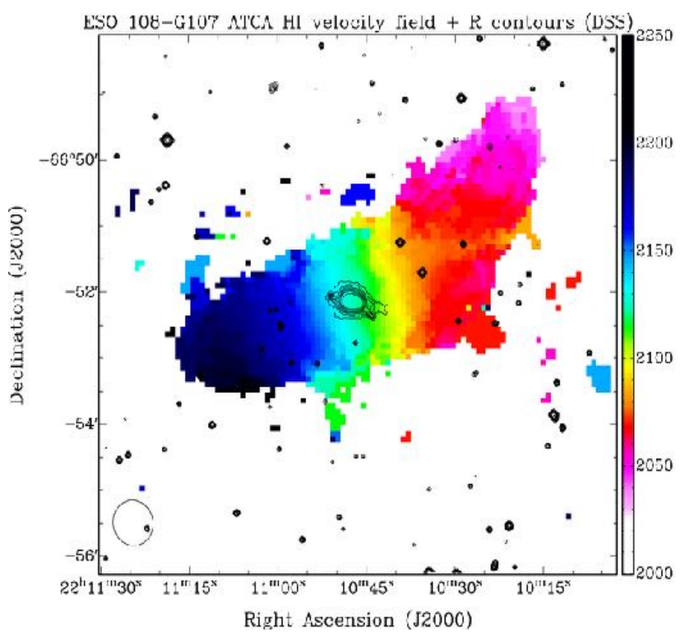

Ángel R. López-Sánchez @El_Lobo_Rayado

MACQUARIE University

KOALA IFU at the Anglo-Australian Telescope

Instrument Scientist: **Ángel R. López-Sánchez**

- **KOALA (Kilofibre Optical AAT Lenslet Array)** is a wide-field, high efficiency, integral field unit (IFU)
- It is mounted at the **f/8 Cassegrain focus** and feeds the **AAOmega spectrograph** via a 31m fibre run.

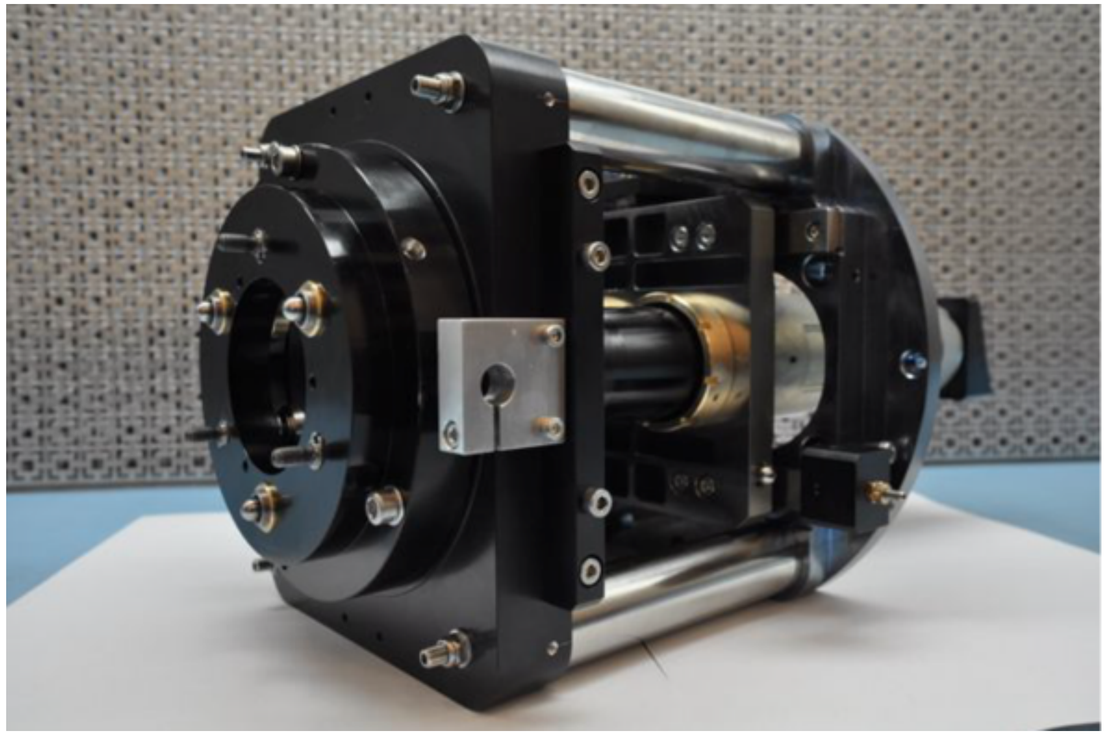

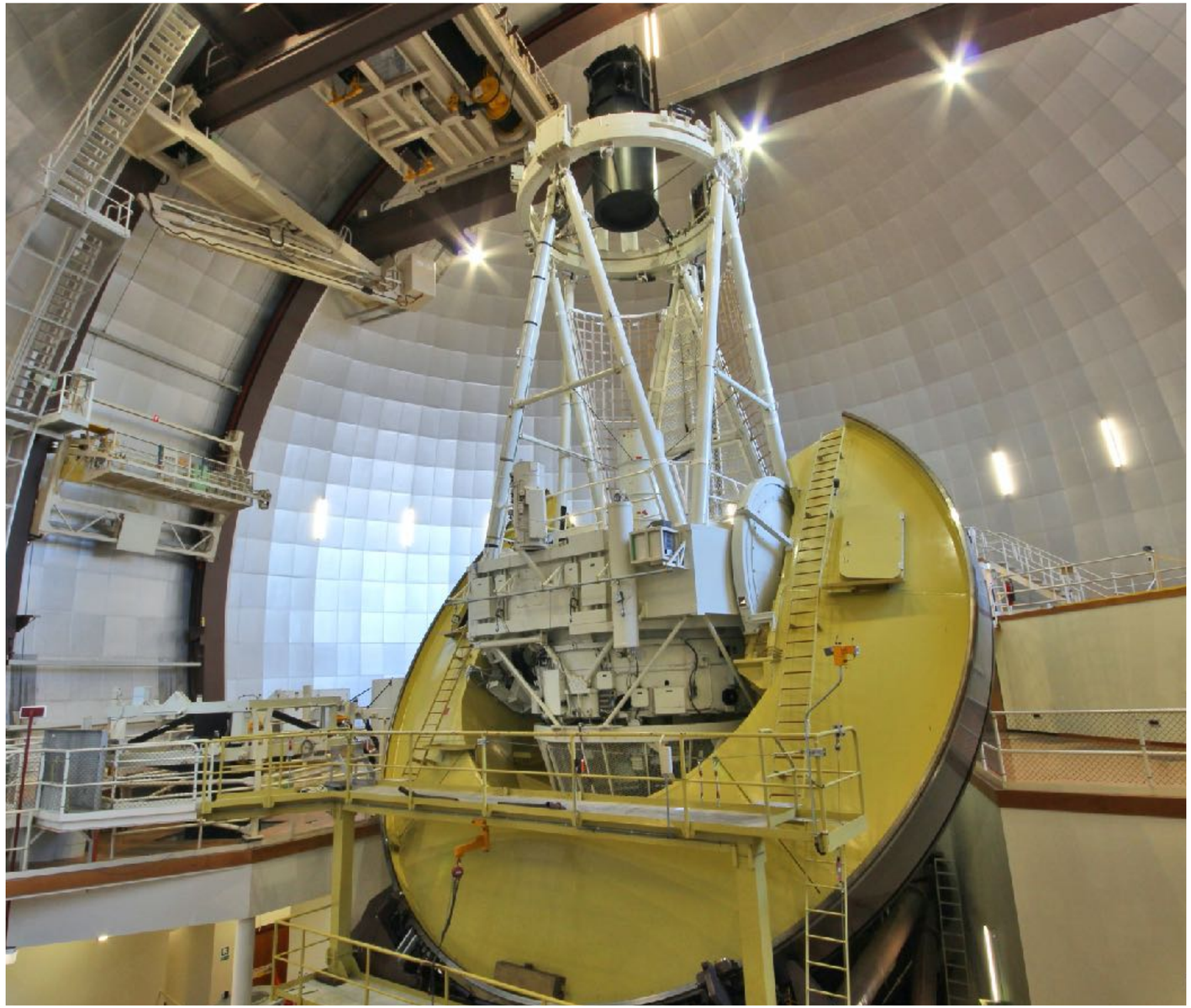

KOALA IFU at the Anglo-Australian Telescope

Instrument Scientist: **Ángel R. López-Sánchez**

- **KOALA (Kilofibre Optical AAT Lenslet Array)** is a wide-field, high efficiency, integral field unit (IFU)
- It is mounted at the **f/8 Cassegrain focus** and feeds the **AAOmega spectrograph** via a 31m fibre run.
- **AAOmega** is a double beam spectrograph with selectable wavelength coverage and resolution.
  - ✓Same spectrograph used for **SAMI**

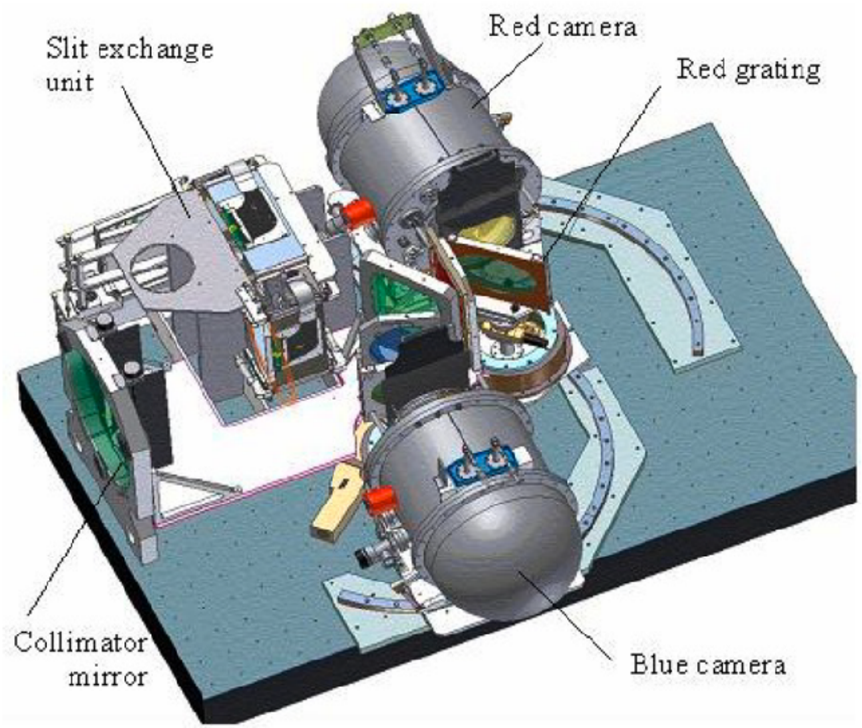

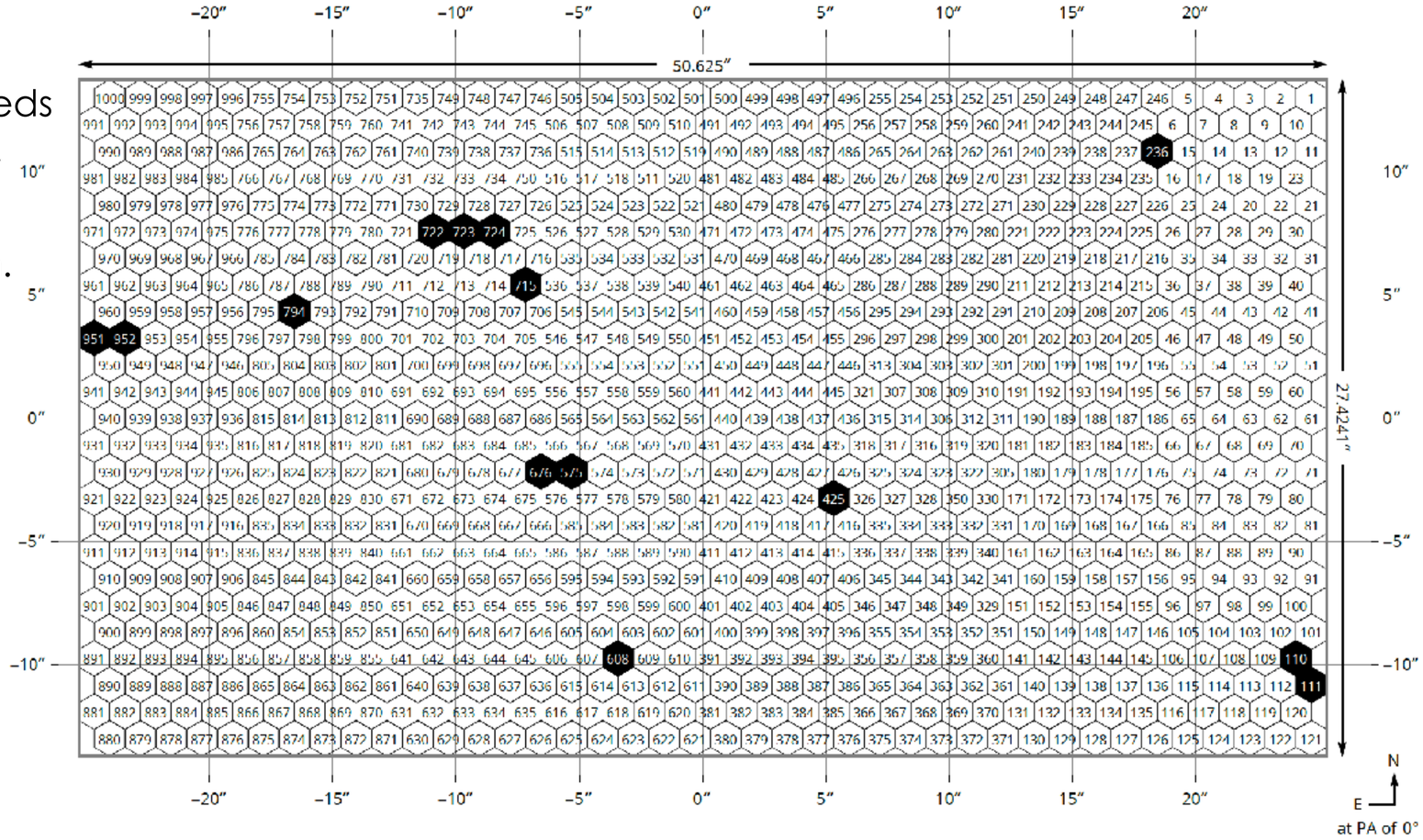

- It has **1000 hexagonal lenslets**
- The field of view is selectable:
  - ✓**15.3" x 28.3"**, with **0.7"** spatial sampling
  - ✓**27.4" x 50.6"**, with **1.25"** spatial sampling

KOALA IFU at the Anglo-Australian Telescope

Instrument Scientist: **Ángel R. López-Sánchez**

- **KOALA (Kilofibre Optical AAT Lenslet Array)** is a wide-field, high efficiency, integral field unit (IFU)
- It is mounted at the **f/8 Cassegrain focus** and feeds the **AAOmega spectrograph** via a 31m fibre run.
- **AAOmega** is a double beam spectrograph with selectable wavelength coverage and resolution.
  - ✓Same spectrograph used for **SAMI**

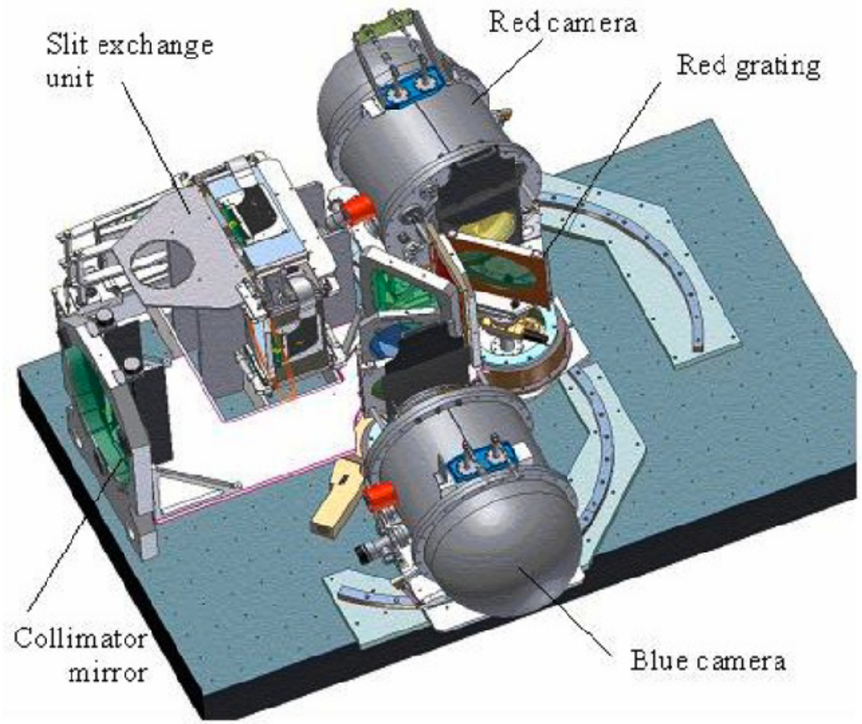

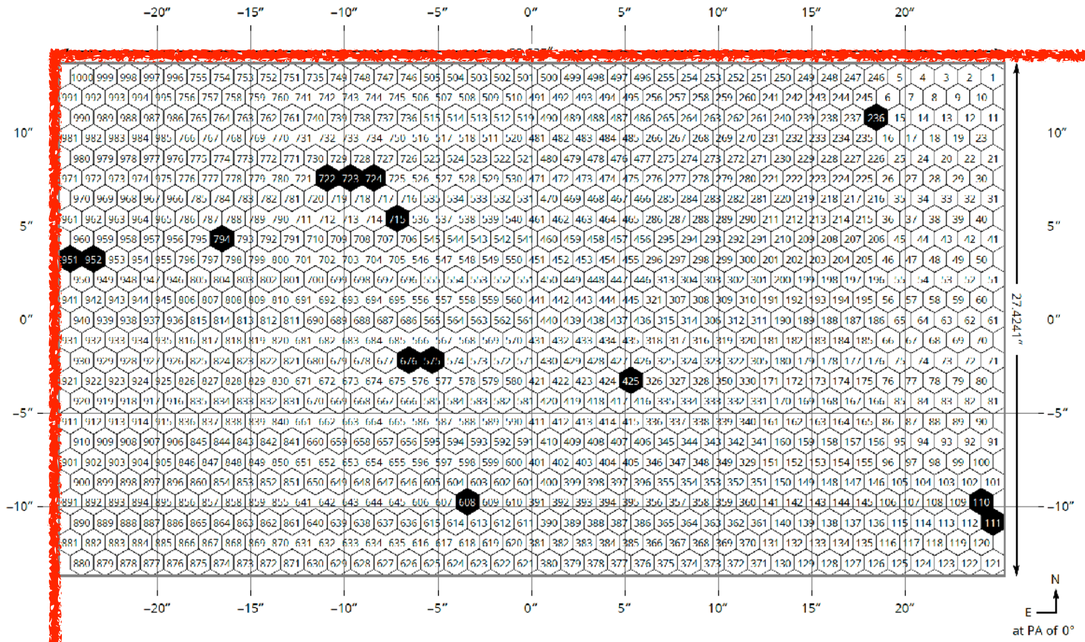

KOALA FoV = 39% MUSE FoV

- It has **1000 hexagonal lenslets**
- The field of view is selectable:
  - ✓**15.3" x 28.3"**, with **0.7"** spatial sampling
  - ✓**27.4" x 50.6"**, with **1.25"** spatial sampling

Hi-KIDS: Observations at the 3.9m Anglo-Australia Telescope

N	Galaxy	Coordinates	Type	mB	Size	Vrad	DATE	Gratings	PA	EXP TIME	POS	RUN	OFFSETS
1	NGC1522	04 06 07.9 -52 40 06	BCDG	13.93	1.2 x 0.8	898	2016 01 16	580V + 1000R	-45	1200	A	47	0 0
								580V + 1000R			B	49	0.812N 0.951W
											C	50	1.646S 1.406W
											A	51	0.834N 2.357E
2	Tol 9	10 34 38.7 -28 35 00	BCDG	14.4	0.7 x 0.4	3190	2016 01 16	580V + 1000R	45?	1200	A	54	0 0
											B	55	0.812N 0.951 W
											C	56	1.646S 1.406W
							2018 02 22	580V + 1000R	135	1800		39-44	CHECK
							2018 02 24	580V + 1000R	135	1800		39-41	
							2018 03 09	580V + 385R	135	1200	a	61	0 0
											b	62	0.88N 0.88E
											d	63	1.53N 1.53W
3	POX 4	11 51 11.6 -20 36 02	BCDG	16.2	0.21 x 0.18	3589	2016 01 16	580V + 1000R	120	1800	A	58	0 0
											B	59	1.189N 0.386E
											D	60	0.669N 2.059W
							2018 03 10	580V + 385R	120	1200	a	91	0 0
											b	92	1.08N 0.62E
											d	93	1.08N 1.88W
4	Mkn 750	11 50 02.7 +15 01 23	BCDG	15.3	0.55 x 0.36	749	2016 01 16	580V + 1000R	135	1800	A	61	0 0
											B	62	1.066N 0.653E
											C	63	1.131N 1.846W
5	Tol 1924-416	19 27 58.2 -41 34 32	BCDG	13.3	0.8 x 0.4	2834	2016 06 29	580V + 385R	0	1800	a	58	0 0
											b	59	1.25W
											d	60	2.165S
							2017 10 13	580V + 385R	0	1200	A	32	0 0
											B	33	1.2N 0.8E
											C	34	0.4S 1.5W
								580V + 1000R	0	1200	C	36	0 0
											B	37	0.4N 1.5W
											A	38	1.2S 0.8W
6	IC 4870	19 37 37.6 -65 48 43	BCDG	13.9	1.6 x 0.9	875	2016 10 22	580V + 1000R	40	1800	a	37	0 0
											b	38	0.735N 1.091W
											d	39	1.752S 1.273W
							2018 04 27	580V + 385R	90	1800	c	38	0 0
											a	39	0.62S 1.08E
							2018 07 06	580V + 385R	40	1800	a	21	0 0
											b	22	0.735N 1.091W
											d	23	1.752S 1.273W
7	ESO 199-G007	02 58 04.2 -49 22 59	dS	16.4	1.0 x 0.4	631	2017 10 13	580V + 1000R	90	1500	A	50	0 0

- Current status:
  - **Almost 100 galaxies observed ! (~300 pointings)**
  - 70 nights so far!
  - **PyKOALA: new Python pipeline to reduce KOALA data!**

  (Still dealing with some details, but we are almost there…)
- We got **MUSE @ VLT** data of a subsample of the galaxies!
  - Observations conducted in P101 and P102.
- The data and derived products will be publicly available in **AAO Data Central**

Ángel R. López-Sánchez @El_Lobo_Rayado

Hi-KIDS: Preliminary results in BCDGs: POX 4

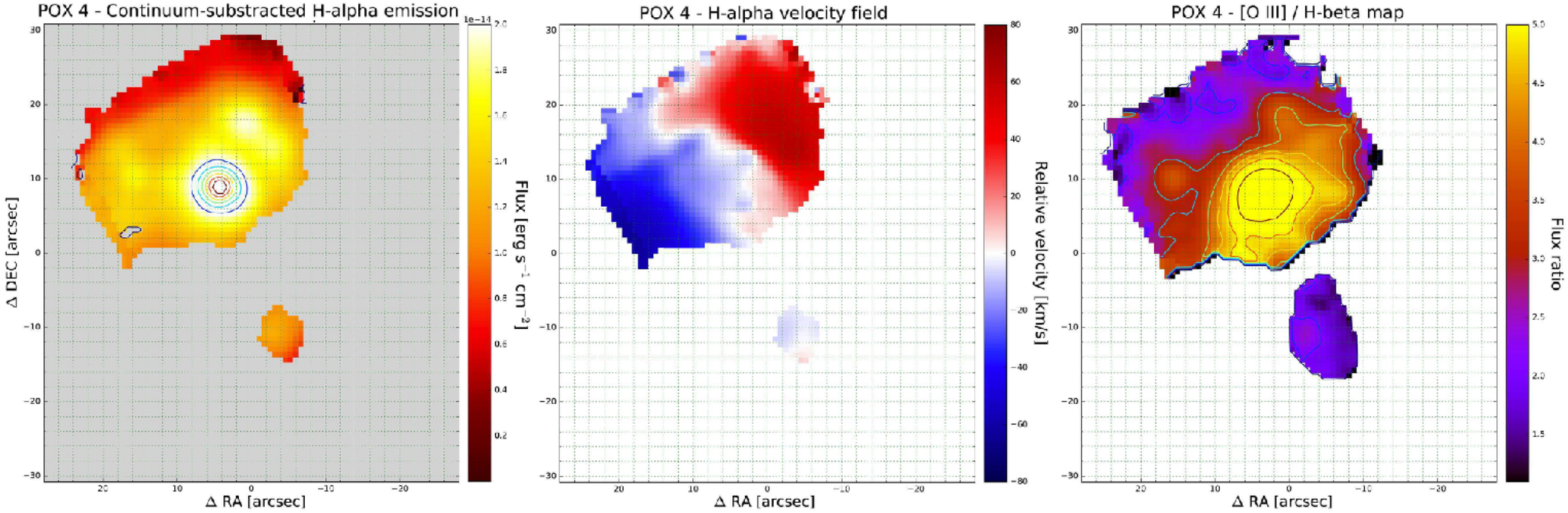

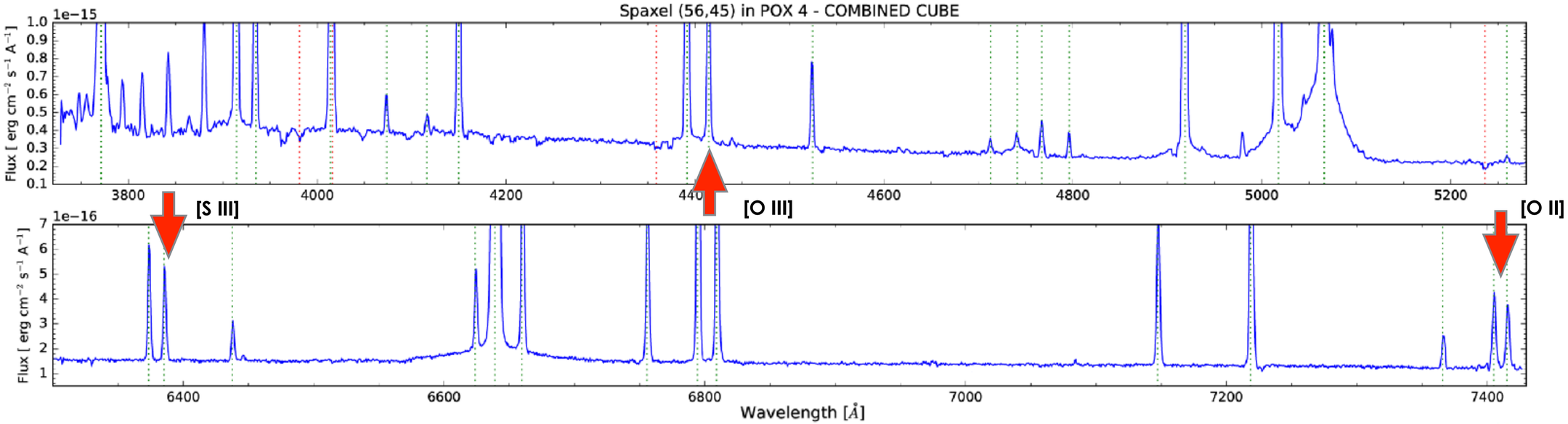

Ángel R. López-Sánchez @El_Lobo_Rayado

Unveiling the nature of starburst dwarf galaxies in HI-KIDS

Adithya Gudalur Balasubramaniam, Dr. Ángel López-Sánchez
Macquarie University

POX 4 is a Blue Compact Dwarf Galaxy observed by HI-KIDS (HI - KOALA IFS Dwarf galaxy Survey) that host a young starburst region in its centre. We propose that the triggering mechanism of the starburst could be the interaction with the companion object (tail).

Starburst regions are seen by the bright spots in the Hα integrated map.

The integrated maps were plotted using Hi-KIDS data obtained with the KOALA integral field unit and the AAOmega spectrograph at the Anglo-Australian Telescope.

Starburst regions help us understand how rapid star formation can affect dwarf galaxies. This can be used to model the impact on much larger galaxies as well.

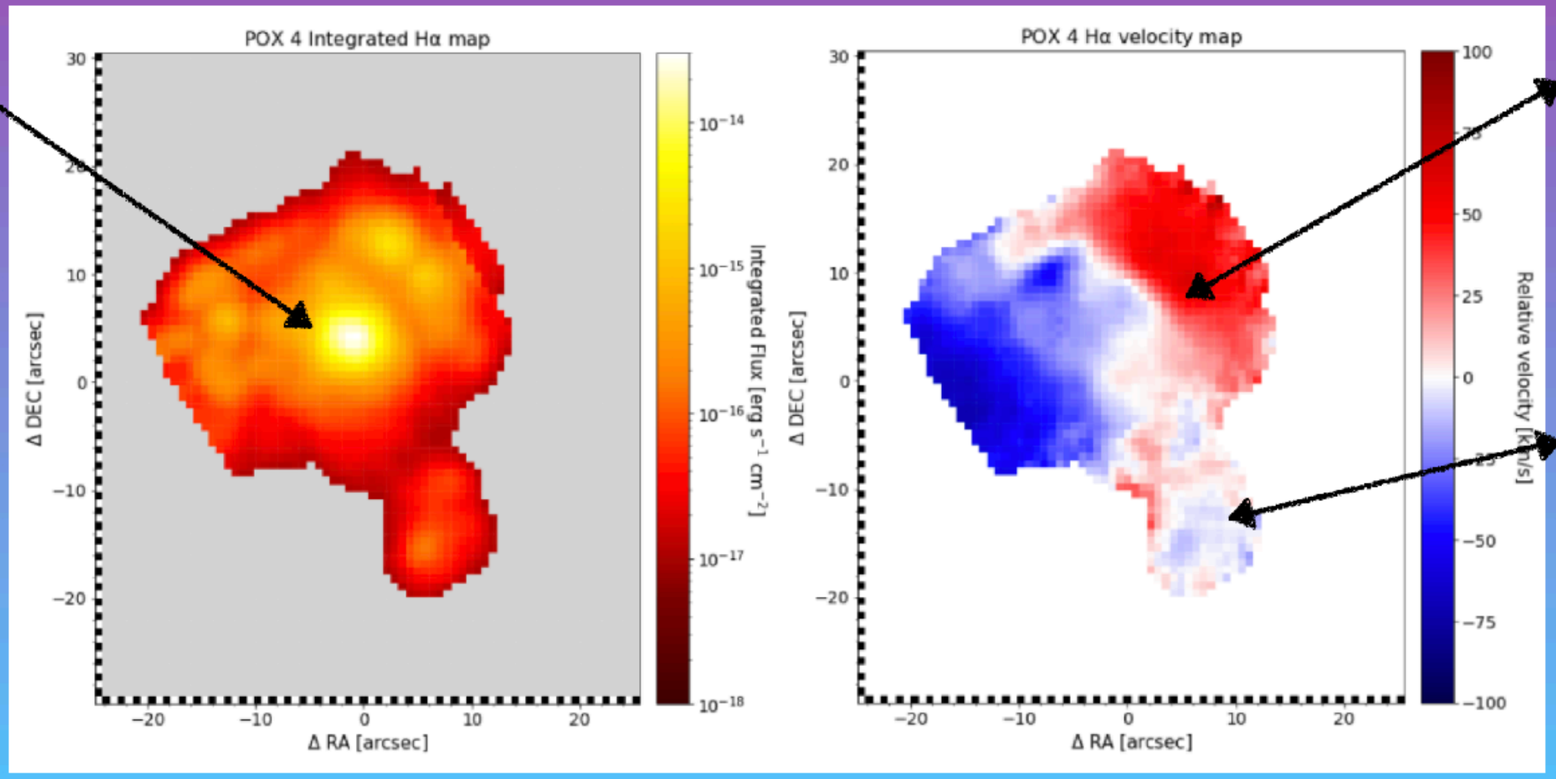

The relative velocity distribution of the gas is very unexpected due to its sinusoidal shape across POX 4.

The presence of the turbulence in the companion object provides some evidence about a potential galaxy interaction.

These interactions could be the reason why POX 4 shows strong starbursts, that has also impacted on the kinematics of the gas in the galaxy.

The KOALA+AAOmega data were processed with the new PyKOALA code (López-Sánchez et al. in prep)

Hi-KIDS as a science case for BlueMUSE

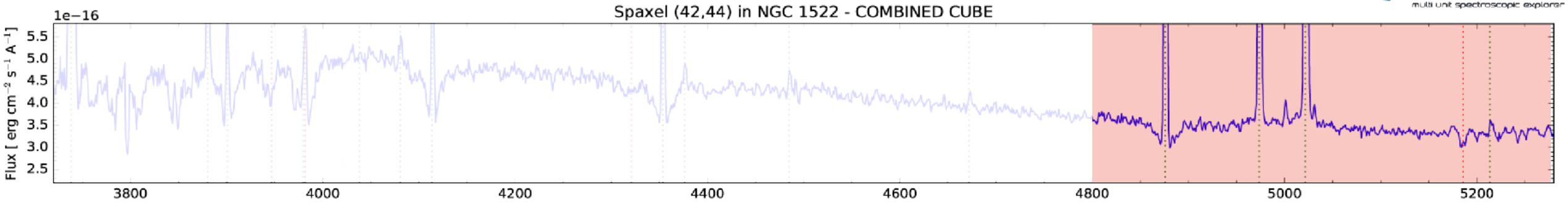

Resolving HII regions, ISM structure, stellar & SF feedback & stellar populations in nearby galaxies

- **Massive stellar content** (fundamental to understand stochastic sampling of the **IMF**, needed for **SFR** & **SFH**).
- Studying **Wolf-Rayet** populations (ionizing sources).
- **Resolved stellar populations** (HI and He absorption lines).
- **HII regions** & **DIG** properties (temperature, densities, ionisation metallicities)using critical **[O II] λ3727 & [O III] λ4363 (Te-method)**
  - > Trace **gas inflows and outflows** !!
  - > **Time scales** for gas inflows and gas mixing.
  - > Exploring the **absolute O/H scale** (+ N, Ne, S, Ar …)
- Understanding **BCDGs**: feeding, processing, feedback.

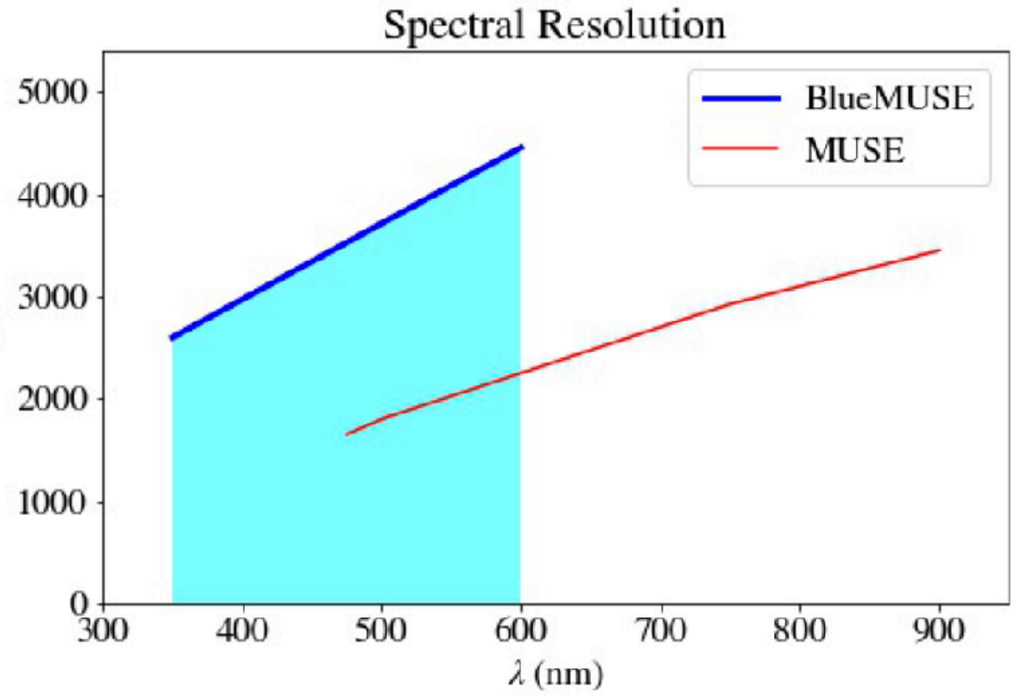

- The power of having **HI gas** (e.g. WALLABY) + **radio continuum** (e.g. EMU) [ideally, also + **CO** (ALMA)].

Ángel R. López-Sánchez @El_Lobo_Rayado